Chemical Engineering Journal 445 (2022) 136782

Contents lists available at ScienceDirect

Chemical Engineering Journal

journal homepage: www.elsevier.com/locate/cej

Simultaneous determination of the position, release time and mass release rate of an unknown gas emission source in short-term emissions by inverse problem

Juan Francisco Sánchez-Pérez [a,*], Gonzalo García-Ros [b], Enrique Castro [a]

[a] Department of Applied Physics and Naval Technology, Area of Applied Physics, Universidad Politécnica de Cartagena (UPCT), Cartagena, Spain
[b] Department of Mining and Civil Engineering, Area of Ground Engineering, Universidad Politécnica de Cartagena (UPCT), Cartagena, Spain

ARTICLE INFO

Keywords:
Gas emission
Inverse problem
Position estimation
Time release and mass rate estimation
Coefficient of deformation by dispersion
Dimensional characterization

ABSTRACT

This article proposes a protocol for the simultaneous determination of the position, release time and mass release rate of an unknown gas emission source from experimental data in the form of an inverse problem, since these are the main variables in the short duration release of pollutants.

Records of pollutant concentration and of measurement time (with their inherent errors) carried out at two measuring stations are the input data for the inverse problem. The actions of the protocol are divided into two well-differentiated stages. In the first, the simulations are started for each iteration, the functionals are calculated to program the next iteration, setting the new values of measurement time and the distance of the emission source in downwind direction with respect to the measuring stations by comparing the simulated and experimental values, and so on until reaching the final solution. In the second, an analogous procedure is followed until the mass rate and the emission source position is obtained. In addition, it has been necessary to define a new coefficient that relates the effect of dispersion in the measurement time, the distance in the downwind direction and the atmospheric stability categories.

The reliability of the proposed protocol is checked by means of a problem whose parameters are known a priori. First, the direct problem is solved to obtain the values of contaminant concentration and the measurement time of the stations. These variables are then affected by random errors of up to 2% to provide the input data for the inverse problem. In all the examples shown in this work, solutions have been obtained that can be considered very successful in this field of engineering.

1. Introduction

The release of chemical compounds into the atmosphere, such as nitrogen or sulfur oxides, particulate matter, carbon monoxide, etc., can be harmful to the health of the population. The atmospheric dispersion of these pollutants depends mainly on the wind speed in the lower layers of the atmosphere, being the study of their behavior an important challenge for environmental engineering [1–3]. The mathematical and/or numerical study of the atmospheric dispersion of pollutants has produced analytical or semi-analytical solutions with increasingly precise results for both continuous and short-term emission [4–10].

Therefore, the emission of certain pollutants can cause harmful effects by increasing the concentration in the area near the emission source, in some cases reaching values higher than those recommended by international organizations. Specifically, when a short duration emission of pollutants occurs, their concentrations increase, which can cause, among others, acute effects [11]. For all the above, it is necessary to develop an inverse problem protocol that allows determining the mass rate, release time and where the pollutant release has occurred, knowing the variables provided by the measuring stations.

The development of the work is as follows. The mathematical model for both the direct and the inverse problems is described, as well as the protocol to implement the inverse problem. Dimensional characterization is applied to establish concentration and distance relationships that will facilitate the development of the inverse problem. Afterward, the direct problem to determine the pollutant concentration and the measurement time for two measuring stations is solved. These variables

* Corresponding author at: Department of Applied Physics and Naval Technology, Area of Applied Physics, Universidad Politécnica de Cartagena (UPCT), Alfonso XIII Avenue, 48, 30203 Cartagena, Spain.
E-mail address: juanf.sanchez@upct.es (J.F. Sánchez-Pérez).

https://doi.org/10.1016/j.cej.2022.136782
Received 29 January 2022; Received in revised form 28 April 2022; Accepted 30 April 2022
Available online 5 May 2022

Nomenclature

C_p	pollutant concentration at a certain position and time (g/m^3)
$C_{p,max}$	pollutant maximum concentration at a certain position and time (g/m^3)
g_y	function of the y coordinate necessary for the calculation of the Gaussian distribution
g_z	function of the z coordinate necessary for the calculation of the Gaussian distribution
h_i	height of the inversion (m)
h_s	height of the emission source (m)
Q	rate of mass release (g/s)
t	time (s)
t_r	pollutant release time (s)
t_r*	starting values for release time (s)
Δt_m	time that the station has been measuring the pollutant (s)
V_x	wind speed in downwind direction (m/s)
x	position in downwind direction (m)
y	position in horizontal crosswind direction (m)
z	position in vertical direction (m)
Δx	relative distance between the station for x-coordinate (m)
Δy	relative distance between the station for y-coordinate (m)
α_i	dispersion coefficients for each of the spatial coordinates, stability categories and roughness
σ_x	dispersion parameter for x-coordinate
σ_y	dispersion parameter for y-coordinate
σ_z	dispersion parameter for z-coordinate
δ	coefficient of dispersion deformation (m)
ξ	random error
χ	gaussian distribution term
Ψ, ϕ	functionals

Subscripts (for others subscripts do not listed, see general nomenclature)

i	refers to dispersion coefficients
position	refers to position
station	refers to measure station
time	refers to time
ξ	related to random error

Superscripts

i = I, II, III,…	referred to each iteration or simulation for the second stage
j = I, II, III,…	referred to each iteration or simulation for the first stage

affected by a random error, thus allowing us to simulate a real scenario, are the input data of the inverse problem whose solution provides the variables to determine. The methodology shown in this work allows to verify that the proposed protocol for the inverse problem leads to reliable and accurate solutions even with errors in the experimental measurements that can be considered as relatively large.

2. Mathematical models of direct and inverse problems

2.1. Direct problem

There are many models to simulate the direct problem where the concentration of a pollutant is determined at different positions and times once it has been emitted from a point source. Most apply simplifications, being able to obtain analytical or semi-analytical solutions of the pollutant dispersion process. To illustrate the methodology of the inverse problem, in this case we will use the well-known mathematical model given by NOAA for the ALOHA software for the direct problem [10], which is one of the most complete, although the procedure could be used for another mathematical model or software that simulates the direct problem [3,12]. This pollutant dispersion model where a short-term release occurs was developed by Palazzi et al. as an extension of the well-known Gaussian puff model, and presented a good agreement between the experimental and calculated data [13].

The mathematical model for the dispersion of neutrally-buoyant pollutants when a short-term emission occurs is collected in equations (1) to (7) [10]. Equation (1), given by Palazzi et al., is based on a Gaussian dispersion model for short duration releases [13], which includes the dispersion parameters for each of the spatial coordinates (σ_x, σ_y and σ_z), a Gaussian distribution term (χ), wind speed in downwind direction (V_x), the pollutant release time (t_r), which is the time that the source is emitting the pollutant, the time since the start of the emission (t), rate of mass release (Q) and the position from the emission source (x, y and z coordinates). Equation (2) is used to calculate the term of Gaussian distribution (χ) from a continuous steady-state point source given by Hanna [14]. Equation (3) is a function of the y coordinate necessary for the calculation of the Gaussian distribution term (χ). Similarly, expression (4) presents a function for the z coordinate. In this case, two equations are presented, one for when there is inversion and another for when there is not. In these equations, the variable h_s represents the height of the emission source and h_i, the height of the inversion [10]. Finally, the dispersion parameters for each of the spatial coordinates are given in equations (5) to (7) [14–16]. These parameters depend on coefficients (α_i) that encompass the stability category and surface roughness factors, Table 1. To better illustrate the problem, the physical scheme of the direct 3-D problem shows in Fig. 1.

Table 1
Values for the coefficients of dispersion parameters [10].

		Stability categories					
Roughness	Coefficient	A	B	C	D	E	F
Both	α_1	0.02	0.02	0.02	0.04	0.17	0.17
	α_2	1.22	1.22	1.22	1.14	0.97	0.97
	α_3	0.22	0.16	0.11	0.08	0.06	0.04
	α_4	0.0001	0.0001	0.0001	0.0001	0.0001	0.0001
Small surface roughness (Rural)	α_5	0.2	0.12	0.08	0.06	0.03	0.016
	α_6	0	0	0.0002	0.0015	0.0003	0.0003
	α_7	0	0	−0.5	−0.5	−1	−1
Large surface roughness (Urban)	α_5	0.24	0.24	0.2	0.14	0.08	0.08
	α_6	0.001	0.001	0	0.0003	0.0015	0.0015
	α_7	0.5	0.5	0	−0.5	−0.5	−0.5

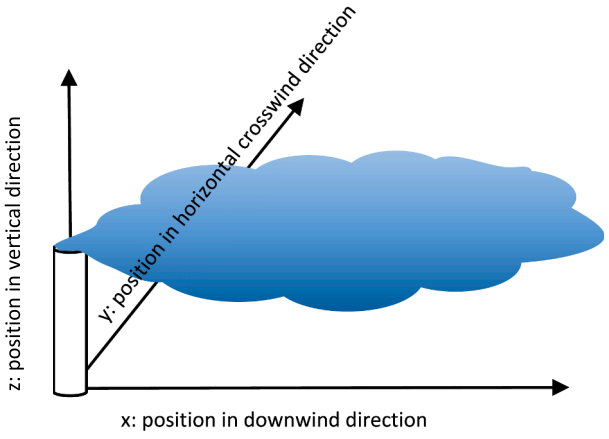

Fig. 1. Scheme of the direct problem.

$$C_p(x,y,z,t) = \frac{\chi}{2}\left[\operatorname{erf}\left(\frac{x}{\sigma_x\sqrt{2}}\right) - \operatorname{erf}\left(\frac{x - V_x t}{\sigma_x\sqrt{2}}\right)\right] \quad \text{for } t \le t_r \tag{1a}$$

$$C_p(x,y,z,t) = \frac{\chi}{2}\left[\operatorname{erf}\left(\frac{x - V_x(t - t_r)}{\sigma_x\sqrt{2}}\right) - \operatorname{erf}\left(\frac{x - V_x t}{\sigma_x\sqrt{2}}\right)\right] \quad \text{for } t > t_r \tag{1b}$$

$$\chi(x,y,z,t) = \frac{Q(t)}{V_x}\, g_y(x,y)\, g_z(x,z) \tag{2}$$

$$g_y(x,y) = \frac{1}{\sigma_y\sqrt{2\pi}} e^{-\frac{1}{2}\left(\frac{y}{\sigma_y}\right)^2} \tag{3}$$

$$g_z(x,z) = \frac{1}{\sigma_z\sqrt{2\pi}}\left(e^{-\frac{1}{2}\left(\frac{z-h_s}{\sigma_z}\right)^2} + e^{-\frac{1}{2}\left(\frac{z+h_s}{\sigma_z}\right)^2}\right) \quad \text{when no inversion is present} \tag{4a}$$

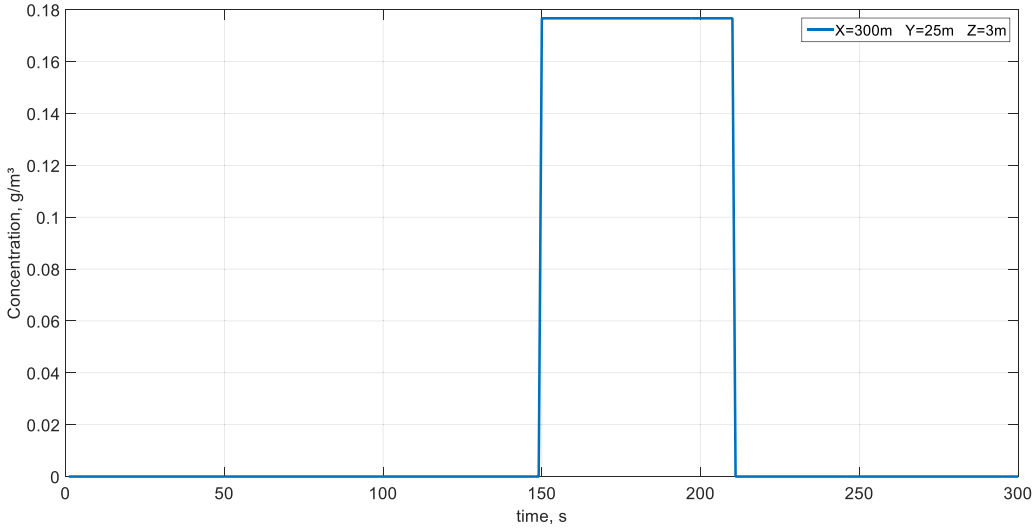

a) Measurement time without dispersion

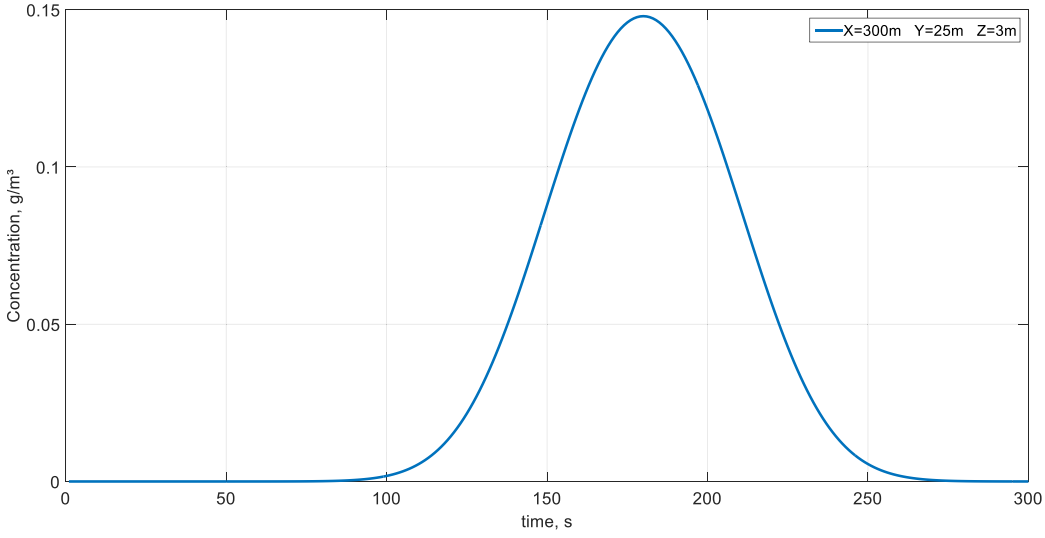

b) Measurement time with dispersion

Fig. 2. Representation of the measurement time of a measuring station with and without dispersion.

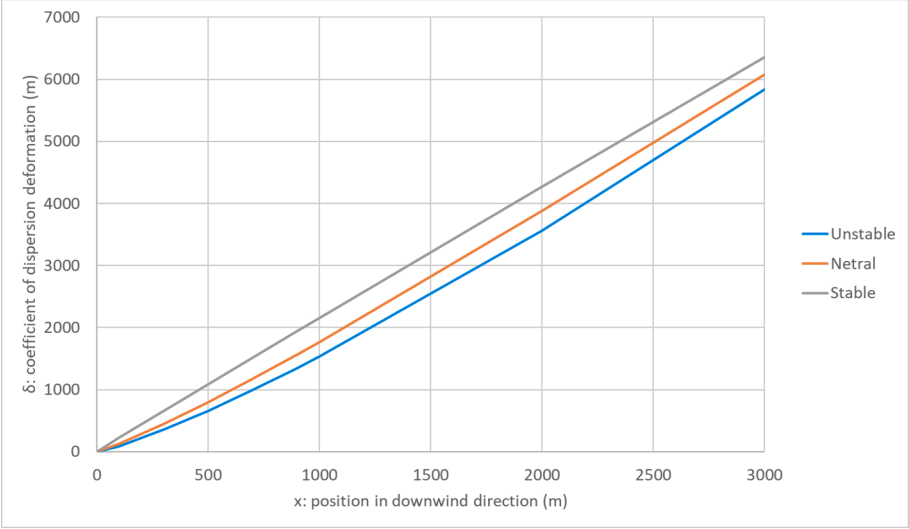

Fig. 3. Representation of the of dispersion deformation (δ) with the distance for each atmospheric stability.

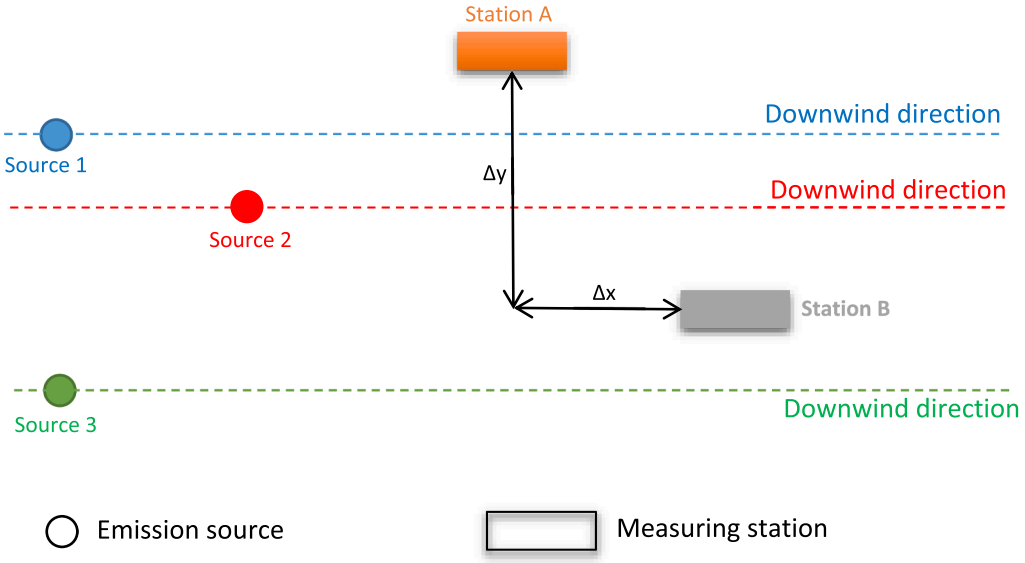

Fig. 4. Projection on the xy-plane of the scenario example for an inverse problem with three emission sources.

$$g_z(x,z) = \frac{1}{\sigma_z\sqrt{2\pi}}\left(e^{-\frac{1}{2}\left(\frac{z-h_s}{\sigma_z}\right)^2} + e^{-\frac{1}{2}\left(\frac{z+h_s}{\sigma_z}\right)^2}\right) + \sum_{n=1}^{j}\left(e^{-\frac{1}{2}\left(\frac{z-2nh_j-h_s}{\sigma_z}\right)^2} + e^{-\frac{1}{2}\left(\frac{z+2nh_j-h_s}{\sigma_z}\right)^2} + e^{-\frac{1}{2}\left(\frac{z-2nh_j+h_s}{\sigma_z}\right)^2} + e^{-\frac{1}{2}\left(\frac{z+2nh_j+h_s}{\sigma_z}\right)^2}\right) \quad \text{when inversion is present} \tag{4b}$$

$$\sigma_x = \alpha_1 x^{\alpha_2} \tag{5}$$

$$\sigma_y = \frac{\alpha_3 x}{\sqrt{1+\alpha_4 x}} \tag{6}$$

$$\sigma_z = \alpha_5 x(1+\alpha_6 x)^{\alpha_7} \tag{7}$$

Equations (1) to (7) of the direct problem have been implemented in a MATLAB® sheet to be able to carry out the simulations of the different cases [17].

2.2. Coefficient of dispersion deformation

If there were no dispersion in the diffusion of atmospheric pollutants, that is, the cloud will behave like a block, an atmospheric pollutant measuring station will measure that pollutant for a time which would coincide with the emission time (Fig. 2a). When there is dispersion, the time that a station measures a contaminant increases with distance, being greater the further away the station is from the emission focus in the downwind direction (Fig. 2b).

In this way, it is possible to define a new coefficient, which we have called coefficient of dispersion deformation (δ), that relates the effect of dispersion in the measurement time of a pollutant, the distance in the downwind direction and the atmospheric stability categories. This coefficient only depends on the distance to the source in the downwind direction, since the other two directions mainly affect the concentration and its influence on the measurement time of the station is practically negligible. In this way we can define the coefficient of deformation by dispersion as:

$$\delta = (\Delta t_m - t_r)V_x \tag{8}$$

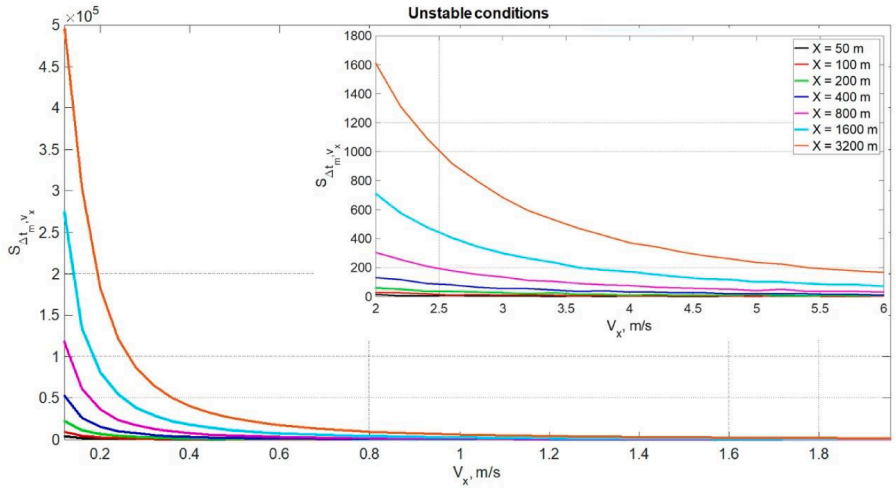

a)

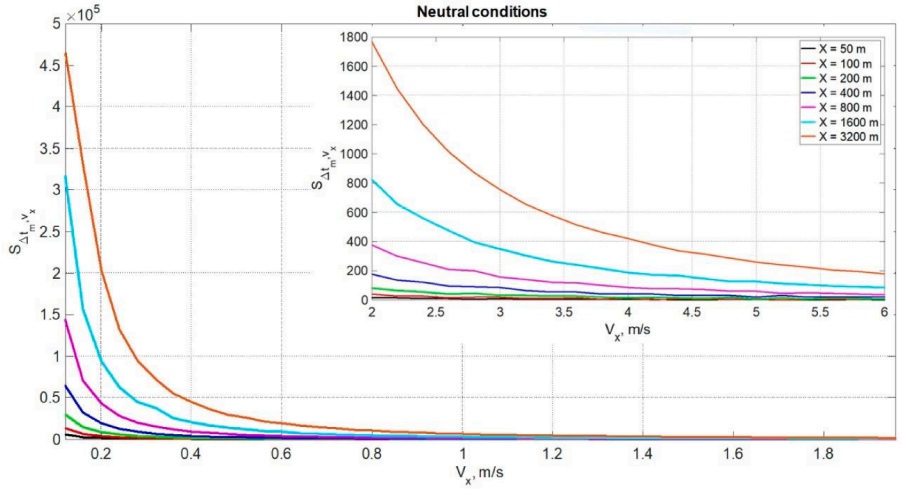

b)

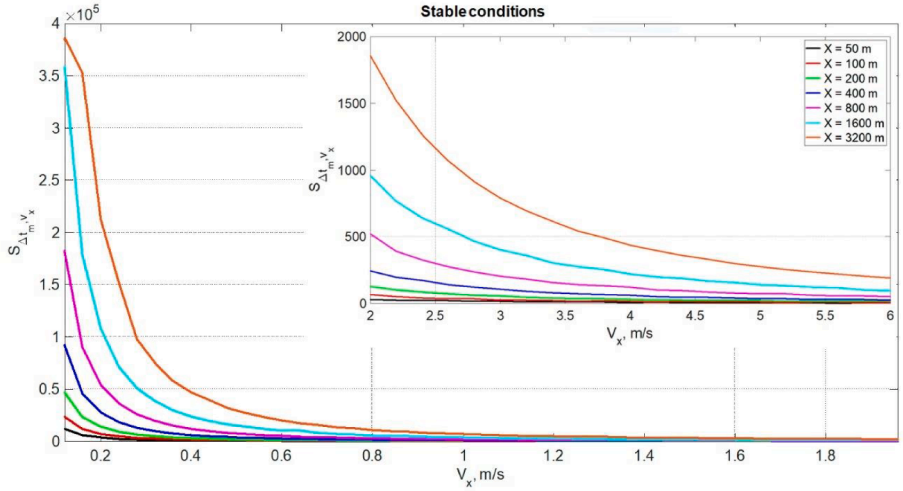

c)

Fig. 5. Sensitivity coefficient $S\Delta_{tm,Vx}$ for different distances and a) unstable, b) neutral and c) stable conditions.

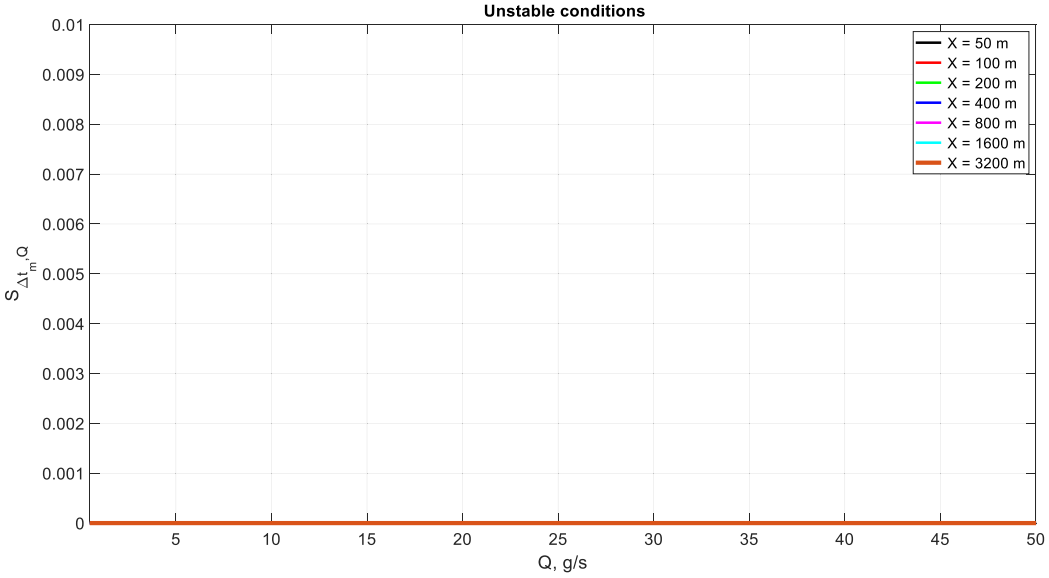

Fig. 6. Sensitivity coefficient $S\Delta_{tm,Q}$ for different distances and unstable conditions.

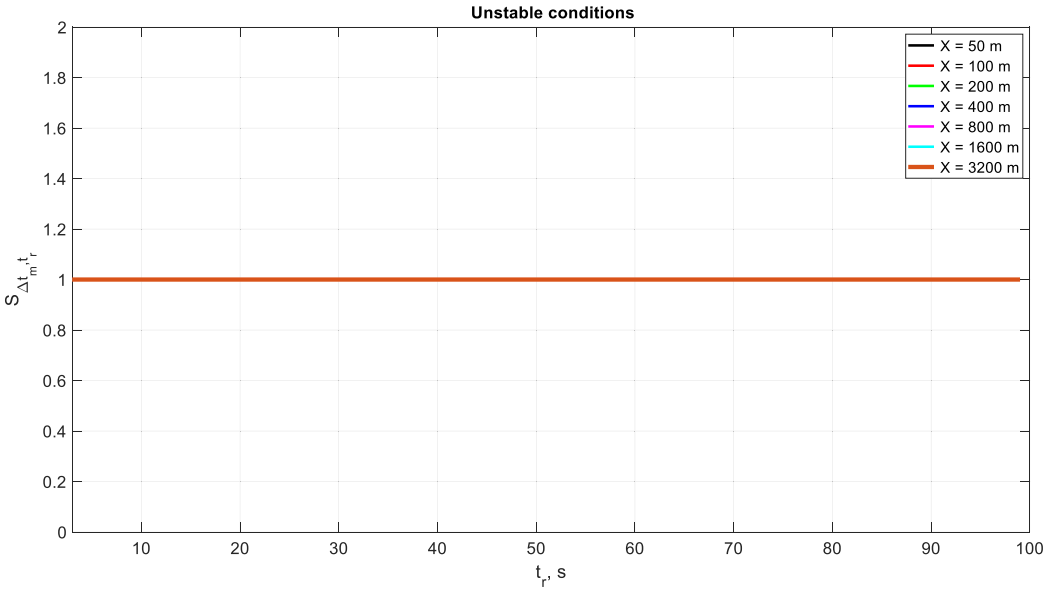

Fig. 7. Sensitivity coefficient $S\Delta_{tm,tr}$ for different distances and unstable conditions.

where Δt_m (s) is the time that the station has been measuring the pollutant. Expression (8) is based on the methodology for the appropriate choice of references to obtain monomials derived from dimensional characterization techniques [18–22]. This methodology is widely used in different engineering problems [23,24].

On the other hand, the categories are grouped in atmospheric stabilities. Thus, categories A, B and C are Unstable, D is Neutral, and E and F are Stable [3,25]. In this way, the coefficients α_1 and α_2 of the dispersion parameter in the downwind direction (σ_x) present the same value for each of the atmospheric stabilities (Table 1). Thereby, if we simulate equations (1) to (7) with a constant speed for different positions in the downwind direction and at ground level, we can represent the coefficient of dispersion deformation (δ), calculated by means of expression (8), against the distance for each of the atmospheric stabilities (Fig. 3) and adjust its trend, equations (9) to (11). It should be noted, derived from the bases of dimensional characterization [19,20,18], these equations are valid for any case, as will be seen later in Section 4.

$$\delta = 0.3348x^{1.220} \quad \text{for unstable conditions} \qquad R^2 = 0.999998 \tag{9}$$

$$\delta = 0.6639x^{1.141} \quad \text{for neutral conditions} \qquad R^2 = 0.999853 \tag{10}$$

$$\delta = 2.3922x^{0.985} \quad \text{for stable conditions} \qquad R^2 = 0.999999 \tag{11}$$

It should be noted that the exponents of expressions (9) to (11) take practically the same values as the exponents (α_2) of the dispersion parameter σ_x for each of the stabilities (Table 1). The differences may be due to the fit of the equations. These equations have been adjusted for a hypothetical measuring station with a sensitivity of $1{\cdot}10^{-20}$ g/m^3. If the

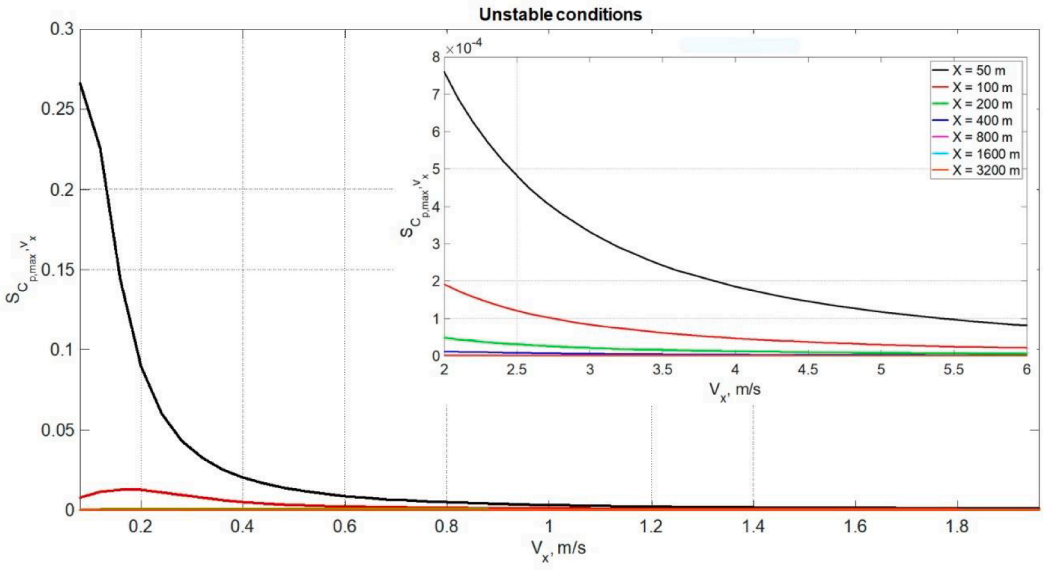

Fig. 8. Sensitivity coefficient $S_{Cp,max,vx}$ for different distances and unstable conditions.

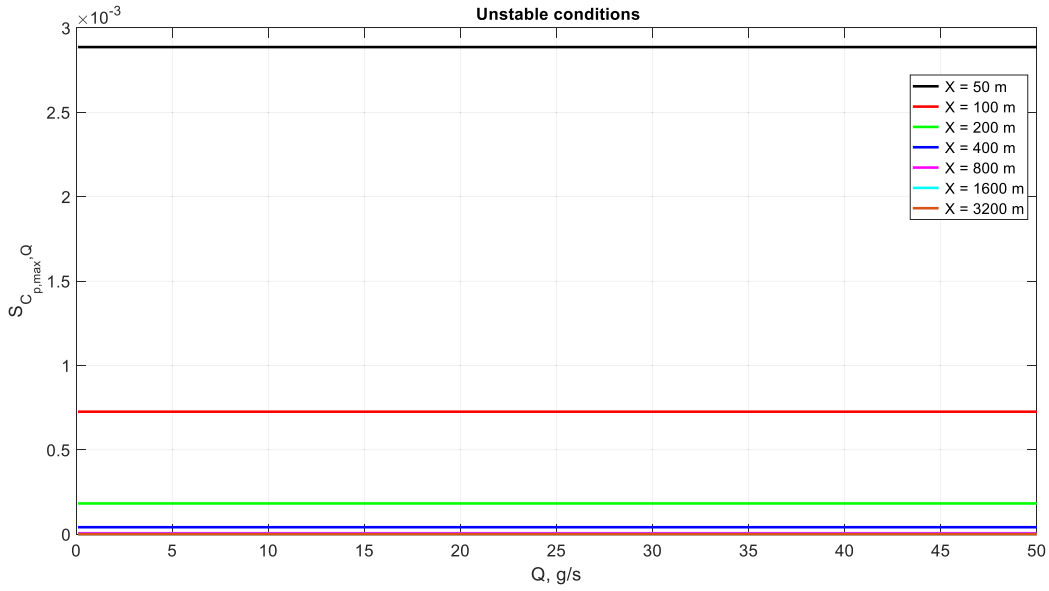

Fig. 9. Sensitivity coefficient $S_{Cp,max,Q}$ for different distances and unstable conditions.

station had a different sensitivity, it would be advisable to adjust the equations for that sensitivity to improve the precision of the methodology proposed in this article.

2.3. Inverse problem

For the scenario of the inverse problem, we have a minimum of two pollutant measuring stations that indicate us the direction and magnitude of the wind, as well as the atmospheric stability obtained by the combination of other environmental parameters, the measurement time and concentration of pollutant. Furthermore, the height of the stations is known as well as the relative distance between them for each direction (Δx and Δy). On the other hand, we know the different possible emission sources from which the instantaneous emission of neutrally-buoyant pollutants has occurred. Fig. 4 shows an example scenario for the inverse problem where there are three emission sources (although there could be more) and two measuring stations. Sources 1 and 3 are at the same distance from the measuring stations in the downwind direction.

The set of governing equations for the inverse problem are the same as for the direct problem plus the equations of the coefficient of dispersion deformation (δ), equations (8) to (11). On the one hand, in this problem, the position of the emission source with respect to the measuring stations, the emission time and the rate of mass release are unknown. By the other hand, the wind speed (V_x) and direction, the atmospheric stability category, the detection time (Δt_m) and maximum concentration of pollutant ($C_{p,max}$) for each station, as well as their relative distance for each direction (Δx and Δy), are known. Solving the inverse problem involves two well-differentiated stages. In the first one, expressions (8) to (11) are used, obtained with dimensional characterization techniques, which allow to easily obtain both the distances from the emission focus to the measuring stations and the release time. In the second, once the position of the emission source is known, the mass

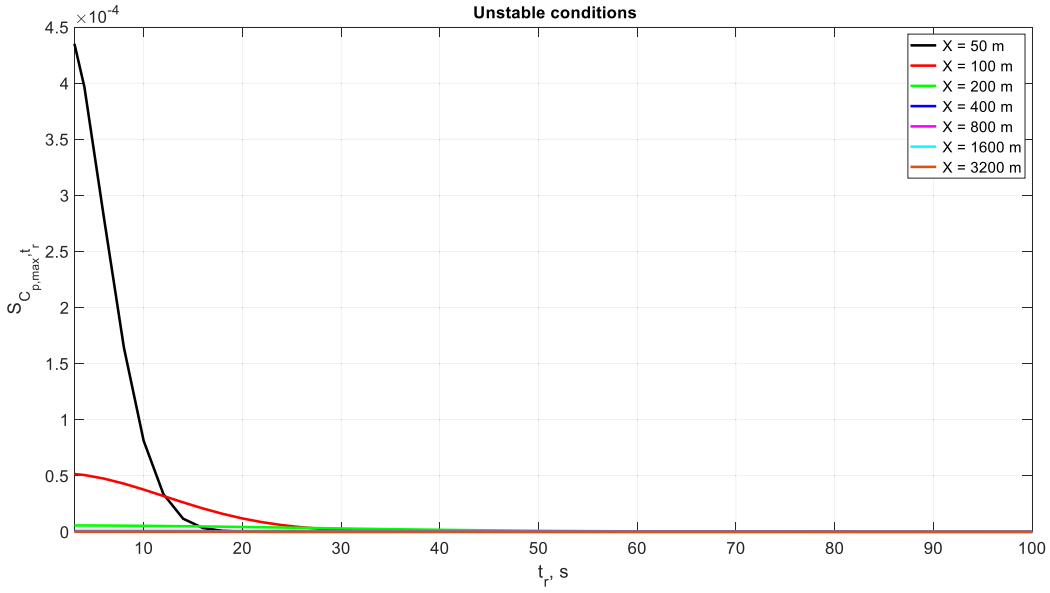

Fig. 10. Sensitivity coefficient $S_{Cp,max,tr}$ for different distances and unstable conditions.

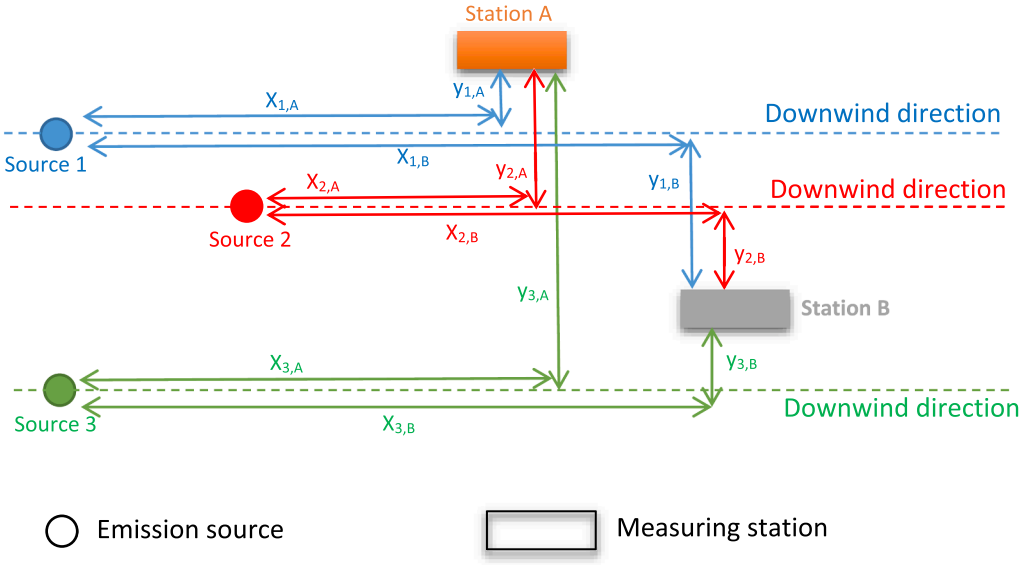

Fig. 11. Projection on the xy-plane of the determination of emission sources located at a distance $x_{A,\xi}$ (or $x_{B,\xi}$) from station A (or B).

release rate is calculated using the direct problem, equations (1) to (7).

The importance of the proposed inverse problem is due to the fact that three of the most important input variables of the direct problem are unknown (the position, the release time and the mass release rate) and it is only known the concentration evolution in an indeterminate time for each of the measuring stations, since the position of the emission source and the release time are not known. In other words, neither when nor the time elapsed since the pollutant release occurred is known, only the time that each of the stations had been measuring the concentration is known.

Finally, to solve the inverse problem, the dimensional characterization methodology supported by more classical techniques is used, such as the implementation of functionals [26–28]. The choice of this methodology instead of other more classic ones such as the Bayesian framework of statistics [29–31], is due to the fact that it has been contrasted in various engineering problems where universal curves have been obtained that allow the resolution of both the direct and the inverse problem with few experimental data, as is the case of the problem under study in this work, since a limited number of experimental data are available, due to the fact that there are only two measuring stations and the emission is of short duration [22,32–34].

2.4. Sensitivity analysis

In choosing the adequate parameters for the inverse problem, the examination of the sensitivity coefficients can provide valuable information, allowing to determine areas of difficulty and improve the proposed procedure. When the coefficients, calculated with the derivative of the dependent variable with respect to a parameter, take small values or are correlated with each other, the estimation of the problem is difficult [26].

This article studies, for different distances and atmospheric stabil-

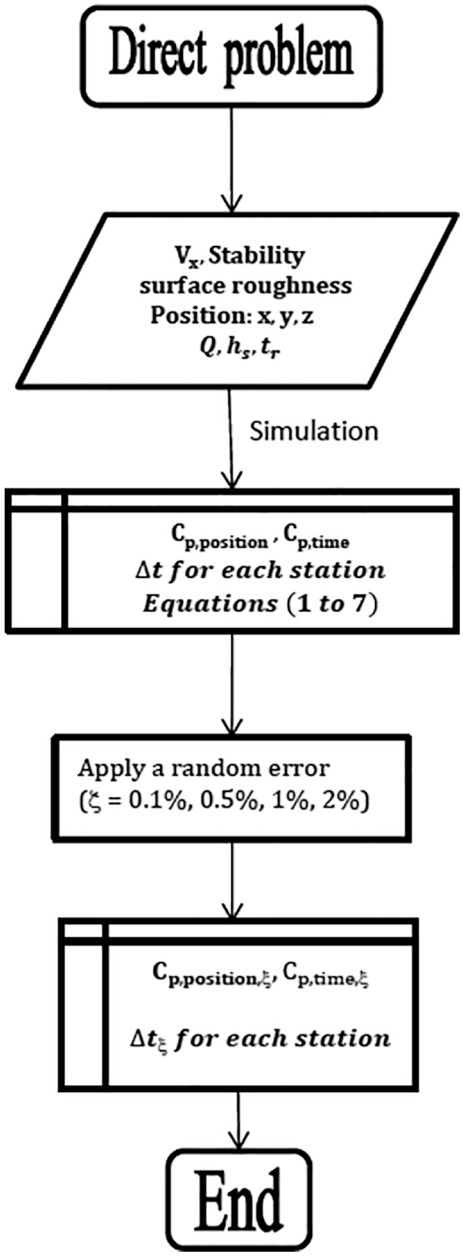

Fig. 12. Flow diagram for the solution of the direct problem.

ities, the sensitivity coefficients of the pollutant maximum concentration ($C_{p,max}$) and the measurement time of the station (Δt_m), since they are the input variables for the inverse problem and are dependent on the wind speed (V_x), the rate of mass release (Q) and the release time (t_r), expressions (12) and (13). When one of the variables changes the rest remains constant, taking the following standard values $V_x = 1$ m/s, $Q = 1$ g/s and $t_r = 100$ s. To calculate the sensitivity coefficients, the direct problem of pollutant diffusion is simulated, equations (1) to (7), implemented in a MATLAB® sheet together with a protocol that calculates the aforementioned coefficients [17]. The value of the sensitivity coefficients is shown in absolute value, since it is only of interest to study its trend and thus its visualization is facilitated.

$$S_{\Delta t_m,V_x} = \left|\frac{\partial \Delta t_m}{\partial V_x}\right| \qquad S_{\Delta t_m,Q} = \left|\frac{\partial \Delta t_m}{\partial Q}\right| \qquad S_{\Delta t_m,t_r} = \left|\frac{\partial \Delta t_m}{\partial t_r}\right| \tag{12}$$

$$S_{C_{p,max},V_x} = \left|\frac{\partial C_{p,max}}{\partial V_x}\right| \qquad S_{C_{p,max},Q} = \left|\frac{\partial C_{p,max}}{\partial Q}\right| \qquad S_{C_{p,max},t_r} = \left|\frac{\partial C_{p,max}}{\partial t_r}\right| \tag{13}$$

First, the sensitivity coefficients of the measurement time of the station are analyzed. If the coefficients related to wind speed are studied (Fig. 5), these take higher values as distance increases, wind speed decreases and atmospheric conditions are more stable. Although as the wind speed increases, the values decrease considerably, they do not take a constant value, that is, they always present a slope. If the sensitivity coefficient is studied through expression (8), proposed for the calculation of the coefficient of dispersion deformation (δ) and obtained by means of dimensional characterization techniques, once rewritten, $\Delta t_m = t_r + \frac{\delta}{V_x}$, it is obtained that the coefficient of sensitivity, $S_{\Delta t_m,V_x} = \left|\frac{\partial \Delta t_m}{\partial V_x}\right| = \left|-\frac{\delta}{V_x^2}\right| \neq 0$, has the same behavior as that obtained by simulation of the direct problem (Fig. 5), validating the previous expression (8). The dependence of the sensitivity coefficient on distance and atmospheric stability is implicitly implemented in the coefficient of dispersion deformation (δ), since it depends on both variables, equations (9) to (11). In conclusion, as the coefficients take large values, the choice of the measurement time of the station, and therefore the coefficient of dispersion deformation (δ) that includes both the wind speed and the measurement time, is a suitable variable and will be used in the first stage of the inverse problem [26]. Regarding the relationship with the rate of mass release, the sensitivity coefficient takes zero value (Fig. 6), which remains constant, so this relationship is not adequate, confirming that it does not appear in the expression of the coefficient of dispersion deformation (δ), since it would take a constant or null value, $S_{\Delta t_m,Q} = \left|\frac{\partial \Delta t_m}{\partial Q}\right| = 0$, as is the case of equation (8). Finally, the relationship between the measurement time and the release time is similar to that of the previous case, but in this case the sensitivity coefficient takes a unit value, which remains constant (Fig. 7). However, this variable appears in the coefficient of dispersion deformation (δ) equation, expression (8), since if it is rewritten $\Delta t_m = t_r + \frac{\delta}{V_x}$, the measurement time depends inversely on the wind speed as a variable, with the release time being the origin ordinate, that is, it takes constant value, so it complies with what was obtained in the sensitivity analysis. That is, if the sensitivity coefficient is studied again through expression (8) rewritten, it is obtained that the coefficient, $S_{\Delta t_m,t_r} = \left|\frac{\partial \Delta t_m}{\partial t_r}\right| = 1$, has the same behavior as that obtained by simulating the direct problem (Fig. 7), validating equation (8) again. As in the last two cases the behavior of the sensitivity coefficients with atmospheric stability is very similar in all conditions, it is only shown as an illustration for unstable conditions (Figs. 6 and 7).

Hereafter, the sensitivity coefficients of the maximum concentration are analyzed. For all the variables, that is, wind speed, rate of mass release and release time, values of the coefficients lower than one are obtained, being more accentuated in the cases of rate of mass release and release time, which present values close to zero in addition to a linear behavior in the case of rate of mass release, making the maximum concentration not a good variable for the inverse problem, so it has been used in the second stage once both the distance from the emission focus to the stations and the release time are known. Again, since the behavior for all atmospheric conditions is similar, it is shown for illustration only for unstable conditions (Figs. 8 to 10).

In conclusion, the sensitivity study confirms the use of expression (8), obtained with dimensional characterization techniques, for calculating the coefficient of dispersion deformation (δ) in the first stage of the inverse problem, as will be shown later, since it implicitly carries the behavior of the measurement time (Δt_m) with the wind speed (V_x), the release time (t_r), the distance and the atmospheric stability. In addition, the expression above also shows the null relationship of the rate of mass release (Q) with the measurement time (Δt_m) derived from the

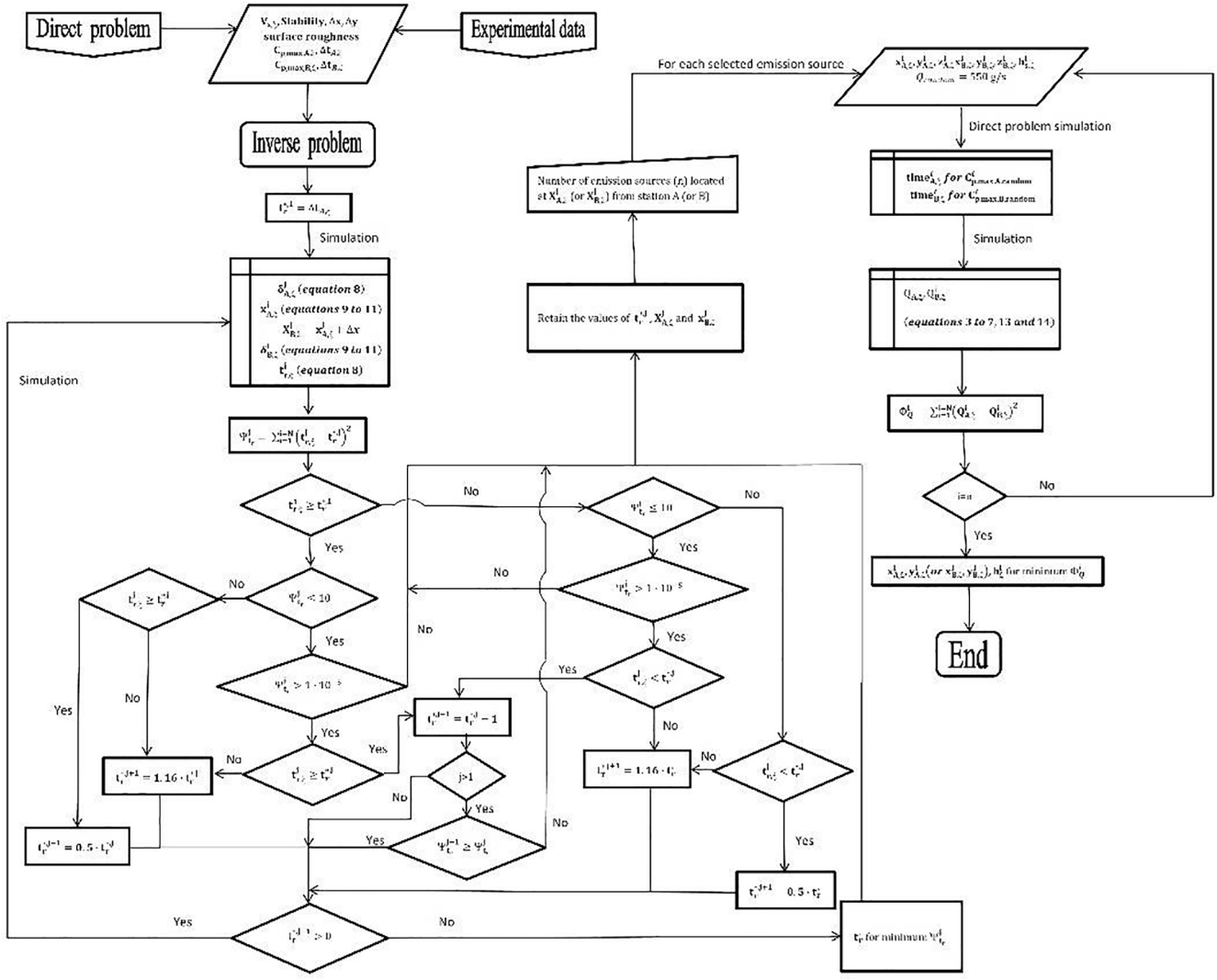

Fig. 13. Flow diagram for the solution of the inverse problem.

Table 2
Input data and results of the direct problem.

Input data for the direct problem														
Source				Atmospheric pollutant measuring station										Roughness
				Station A			Station B			Δx (m)	Δy (m)	V_x (m/s)	Atmospheric stability	
Number	h_s (m)	Q (g/s)	t_r (s)	x (m)	y (m)	z (m)	x (m)	y (m)	z (m)					
1	8	200	360	900	15	0	1500	25	0	600	40	3	A	Rural
Result for the direct problem														
Station A										Station B				
$C_{p,max}$ (g/m^3)				Δt_m (s)						$C_{p,max}$ (g/m^3)				Δt_m (s)
$6.19 \cdot 10^{-4}$				808						$2.29 \cdot 10^{-4}$				1196

aforementioned study. Thus, in this first stage distances from the emission focus to the stations and the release time (t_r) are determined, only missing for the second stage the rate of mass release (Q), since it does not present adequate values in the sensitivity coefficients. On the other hand, the sensitivity study also confirms the use of the maximum concentration in the second stage of the inverse problem, once the distances from the emission focus to the stations and the release time are known, because it is not an adequate variable for the first stage, being used, in the second, in an only step for each of the possible emission sources to calculate the rate of mass release (Q), since the rest of the unknowns are known. Previously, in this second stage, the time in which the maximum concentration is reached for each station is calculated with the direct problem, using a random rate of mass release value, since the time in which this concentration is detected is the same, as derived from the sensitivity study as it depends mainly on wind speed, release time, distance, and atmospheric stability.

3. Protocol for the solution of the inverse problem

The protocol of the inverse problem is constituted by the following steps iv) to xxviii). Additionally, steps i) to iii) are added to be able to verify the proposed protocol by comparing the results of the inverse

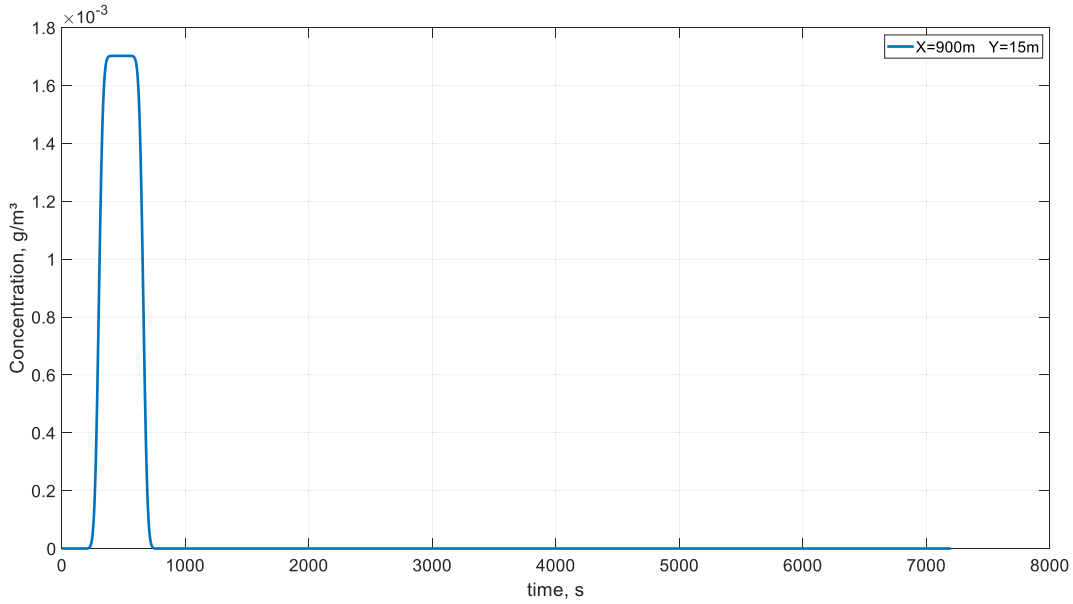

Fig. 14. Evolution of concentration at measuring station A.

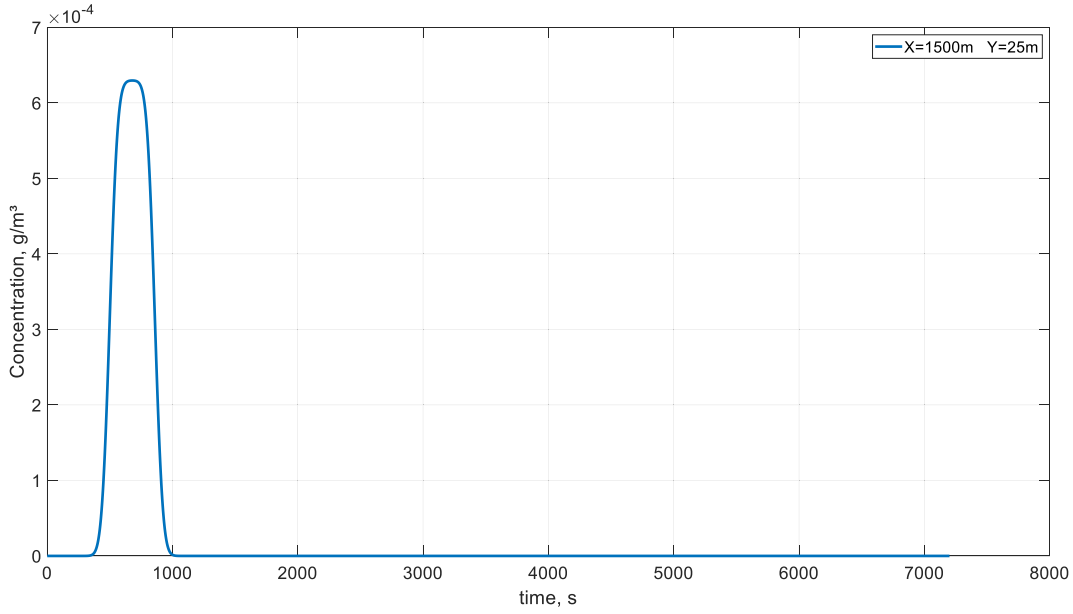

Fig. 15. Evolution of concentration at measuring station B.

Table 3
Height and distance of each of the emission sources to the measuring stations.

	Station A		Station B		h_s (m)
Source	x (m)	y (m)	x (m)	y (m)	
1	900	15	1500	25	8
2	500	30	1100	10	9
3	900	60	1500	20	6

problem with exact and known values. This is a procedure that has been used in numerous works [35–37].

To validate the protocol of the inverse problem, instead of using experimental tests, we will use as input data for the inverse problem the results obtained by simulating the direct problem affected by a random error, which will allow us to compare the results obtained in the inverse problem with the variables introduced in the direct problem. These steps are:

i) The direct problem for the diffusion of pollutants is simulated by defining the wind speed, stability, surface roughness, the height of the emission, the release time and rate of mass release, and finally, the positions of the measuring stations. The time for the simulation must be long enough so that the contaminant can be measured by the station showing an evolution of the contaminant as in the Fig. 2b.

ii) The evolution and distribution profiles of the concentration are obtained ($C_{p,position}$ and $C_{p,time}$), as well as the $\Delta t_{m,station}$ value for each station. It should be noted that for the inverse problem we only need the maximum concentration measured in each station ($C_{p,max,station}$).

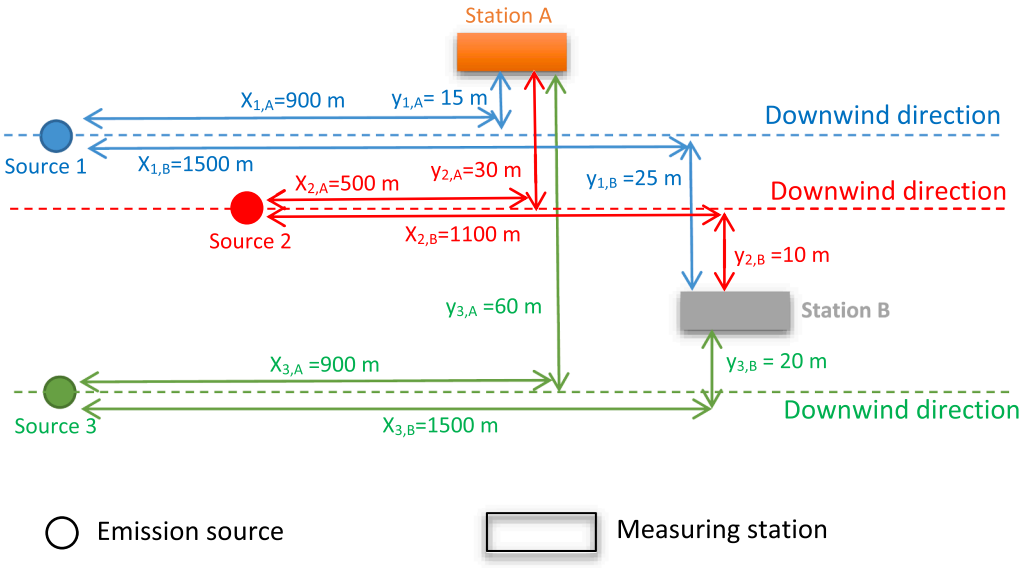

Fig. 16. Projection on the xy-plane of the determination of emission sources located at a distance $x_{A,\xi}$ (or $x_{B,\xi}$) from station A (or B) for the first scenario.

Table 4
Input data or "experimental measurements" obtained from measuring stations. Maximum error of 2%.

Station A		Station B		$\Delta x_{,\xi}$ (m)	V_x (m/s)	Atmospheric stability	Roughness
$C_{p,max,,\xi}$ (g/m^3)	$\Delta t_{m,\xi}$ (s)	$C_{p,max,,\xi}$ (g/m^3)	$\Delta t_{m,\xi}$ (s)				
$6.31\cdot10^{-4}$ (1.94%)	811 (0.37%)	$2.32\cdot10^{-4}$ (1.31%)	1199 (0.25%)	598 (0.33%)	3	A	Rural

Table 5
$x^j_{A,\xi}$, $x^j_{B,\xi}$, $t_r^{*,j}$ and Ψ^j_{tr} for selected iterations.

Iteration	$t_r^{*,j}$ (s)	$t^j_{r,\xi}$ (s)	$x^j_{A,\xi}$ (m)	$x^j_{B,\xi}$ (m)	Ψ^j_{tr}
1	811.00	926.57	0.00	598.00	13356.31
2	405.50	412.15	828.49	1426.49	44.24
–	–	–	–	–	–
11	363.11	364.55	898.84	1496.84	2.09
12	**362.11**	**363.44**	**900.48**	**1498.48**	**1.77**
–	–	–	–	–	–
23	**351.11**	**351.14**	**918.53**	**1516.53**	**0.0012**

iii) A random error ($\xi = 0.1\%, 0.25\%, 0.5\%, 2\%\ldots$, according to the accuracy of the experimental measurements) is applied to the maximum concentration measured at each station ($C_{p,max,station,\xi}$), to the distance between stations (Δx_ξ) and to the time the stations have been measuring the contaminant ($\Delta t_{m,station,\xi}$). To apply the desired random error, for example up to 2%, an Excel® routine with the random function has been used, which generates random numbers using the Mersenne Twister algorithm [38]. We assume that these values affected with an error are equivalent to those obtained by experimental measurements.

iv) The inverse problem has been divided into two stages. In the first, the release time and the distance of the emission source in downwind direction (x) with respect to the measuring stations will be determined. In the second, the rate of mass release and the position of the emission source will be obtained. The input data for the first stage is provided by the measuring stations. Among these stand out: $V_{x,\xi}$, stability, surface roughness, Δx_ξ, $\Delta t_{m,A,\xi}$ and $\Delta t_{m,B,\xi}$.

v) Set starting values for release time ($t_r^{*,j}$). For the initial value, the shortest measurement time of the stations is taken (Δt_m), that is, the time of the station closest to the emission source ($t_r^{*,1} = \Delta t_{m,A,\xi}$), since it has a lower dispersion and therefore, this value will be closer to the release time ($t_r^{*,j}$), as explained in Subsection 2.2.

vi) From the simulation of equations (8) to (11) and using the expression $x^j_{B,\xi} = x^j_{A,\xi} + \Delta x$, is obtained the position of the emission source in downwind direction (x) for each measuring station and the release time ($t^j_{r,\xi}$). The procedure used is the following. First, $\delta^j_{A,\xi}$ is obtained with $t_r^{*,j}$ (equation (8)), and then $x^j_{A,\xi}$ (equations (9) to (11)). The expression $x^j_{B,\xi} = x^j_{A,\xi} + \Delta x$ is used to obtain $x^j_{B,\xi}$, which allows us to calculate $\delta^j_{B,\xi}$ (equations (9) to (11)). Finally, $t^j_{r,\xi}$ is obtained (equation (8)).

vii) Determine the value of the following functional $\left(\psi^j_{t_r}\right)$ given by equation (14), and then, if $t^1_{r,\xi} \geq t_r^{*,1}$, go to step viii), otherwise, go to step xiv).

$$\psi^j_{t_r} = \sum_{i=1}^{i=N} \left(t^j_{r,\xi} - t_r^{*,j}\right)^2 \tag{14}$$

viii) If $\psi^j_{t_r} \leq 10$, go to step ix). If $\psi^j_{t_r} > 10$, go to step xiii).

ix) If $\psi^j_{t_r} > 1\cdot10^{-5}$, go to step x), otherwise, go to step xxi).

x) If $t^j_{r,\xi} \geq t_r^{*,j}$, go to step xi). If it is not meet, apply the expression $t_r^{*,j+1} = 1.16\cdot t_r^{*,j}$ and go to step xx).

xi) Apply the equation $t_r^{*,j+1} = t_r^{*,j} - 1$, and then, if it is the first simulation (j = 1) go to step xx), otherwise, go to step xii).

xii) If the condition $\psi^{j-1}_{t_r} \geq \psi^j_{t_r}$ is met, go to step xx). Otherwise, go to step xxi).

xiii) If $t^j_{r,\xi} \geq t_r^{*,j}$, apply the expression $t_r^{*,j+1} = 0.5\cdot t_r^{*,j}$, otherwise, apply the equation $t_r^{*,j+1} = 1.16\cdot t_r^{*,j}$. Go to step xx).

xiv) If $\psi^j_{t_r} \leq 10$, go to step xv), otherwise, go to step xix).

xv) If $\psi^j_{t_r} > 1\cdot10^{-5}$, go to step xvi). If it is not meet, go to step xxi).

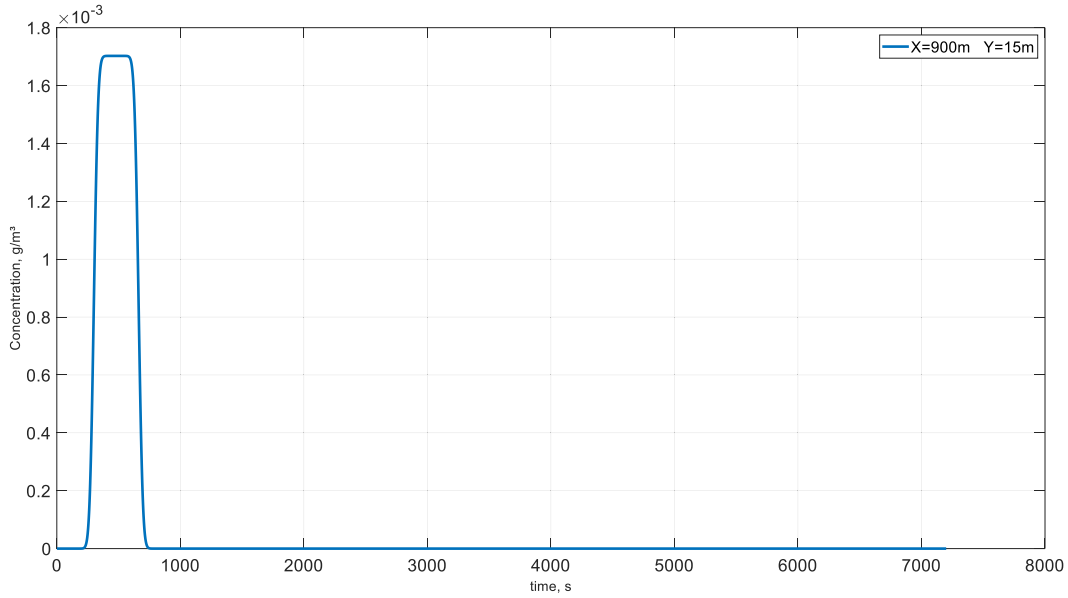

a)

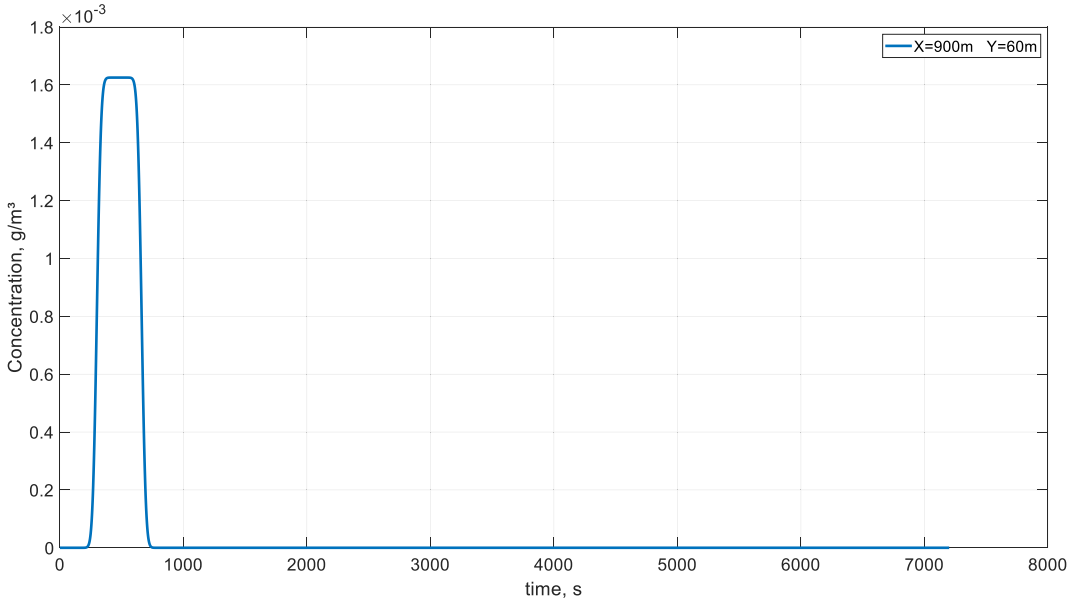

b)

Fig. 17. Evolution of concentration at measuring station A to determine the time at which the maximum concentration occurs for a) source 1 and b) source 3.

xvi) If $t^{i}_{r,\xi} < t^{*,j}_{r}$, go to step xvii), otherwise, apply the expression $t^{*,j+1}_{r} = 1.16 \cdot t^{*,j}_{r}$ and go to step xx).

xvii) Apply the equation $t^{*,j+1}_{r} = t^{*,j}_{r}$- 1, and if it is the first simulation (j = 1) go to step xx), otherwise, go to step xviii).

xviii) If the condition $\psi^{i-1}_{t_r} \geq \psi^{i}_{t_r}$ is met, go to step xx). Otherwise, go to step xxi).

xix) If $t^{i}_{r,\xi} < t^{*,j}_{r}$, apply the expression $t^{*,j+1}_{r} = 0.5 \cdot t^{*,j}_{r}$, otherwise, apply the equation $t^{*,j+1}_{r} = 1.16 \cdot t^{*,j}_{r}$. Go to step xx).

xx) If the new value of $t^{*,j+1}_{r}$ is greater than zero ($t^{*,j+1}_{r} > 0$), go to step vi). Otherwise, choose the value of $t^{*,j}_{r}$ for the minimum value of the functional $\psi^{i}_{t_r}$ and then go to step xxi).

xxi) Retain the values of t_r*, $x^{j}_{A,\xi}$ and $x^{j}_{B,\xi}$, and go to step xxii).

xxii) In this step the second stage begins. Determine the number of emission sources (n) that are located at a distance $x^{j}_{A,\xi}$ (or $x^{j}_{B,\xi}$) from station A (or B), Fig. 11. Go to step xxiii).

xxiii) For each selected emission source $x^{i}_{A,\xi}$, $y^{i}_{A,\xi}$, $z^{i}_{A,\xi}$, $x^{i}_{B,\xi}$, $y^{i}_{B,\xi}$, $z^{i}_{b,\xi}$ and $h^{i}_{s,\xi}$ is known (Fig. 11) and steps xxiv) to xxvi) must be applied. As the

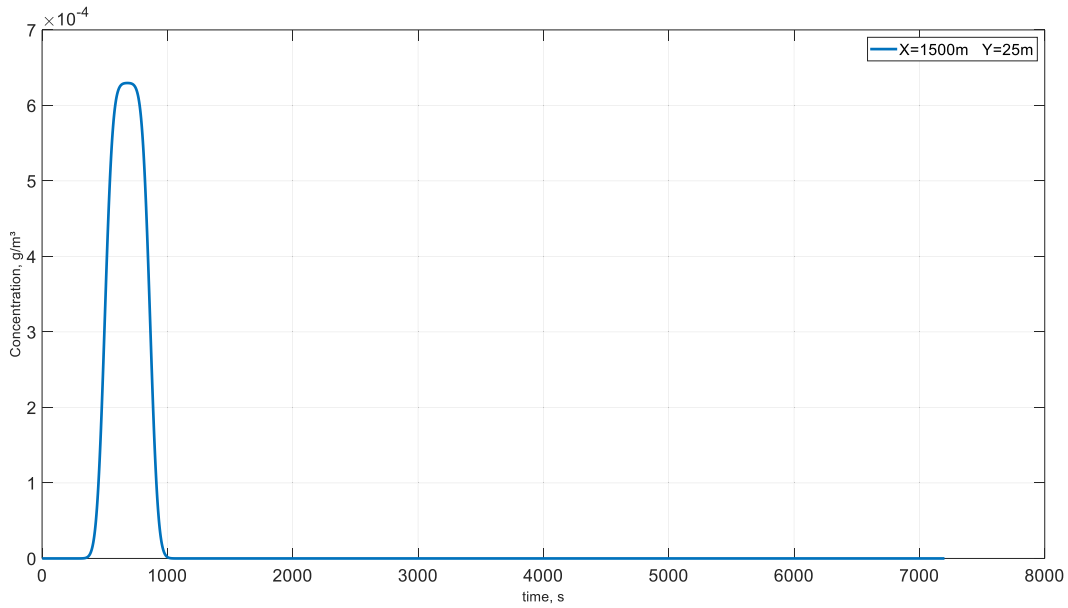

a)

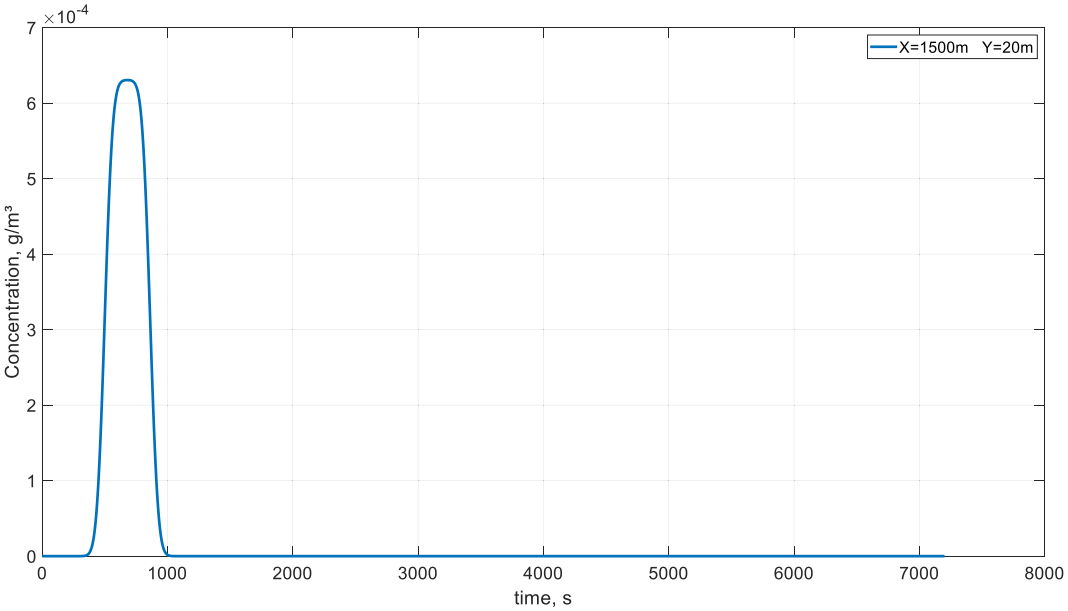

b)

Fig. 18. Evolution of concentration at measuring station B to determine the time at which the maximum concentration occurs for a) source 1 and b) source 3.

Table 6
$Q^i_{A,\xi}$, $Q^i_{B,\xi}$, ϕ^i_Q and $Q^i_{Mean,\xi}$ for sources 1 and 3.

Source	$Q^i_{A,\xi}$ (g/s)	$Q^i_{B,\xi}$ (g/s)	ϕ^i_Q	$Q^i_{Mean,\xi}$ (g/s)
1	203.85	202.66	1.43	203.25
3	213.55	202.38	124.69	207.97

rate of mass release is not known, a random one is taken, for example $Q_{Random} = 550$ g/s, since the time that the maximum concentration is detected in each station is the same although the concentration is different. Go to step xxiv).

xxiv) Simulation of the direct problem (equations (1) to (7)) and determination of the time in which it reaches the maximum concentration value for each station ($time^i_{station,\xi}$ for $C^i_{p,max,station,Q=Random}$). Go to step xxv).

Table 7
Comparison between the results obtained by the direct and inverse problem.

Source	Station A			Station B			h_s (m)	Direct problem		Inverse problem	
	x (m)	y (m)	z (m)	x (m)	y (m)	z (m)		Q (g/s)	t_r (s)	Q (g/s)	t_r (s)
1	900	15	0	1500	25	0	8	200	360	203.25 **(1.63%)**	362 **(0.56%)**

Table 8
Input data and results of the direct problem.

Input data for the direct problem													
Source				Atmospheric pollutant measuring station						Δx (m)	Δy (m)	V_x (m/s)	Atmospheric stability	Roughness
				Station A			Station B							
Number	h_s (m)	Q (g/s)	t_r (s)	x (m)	y (m)	z (m)	x (m)	y (m)	z (m)					
3	12	600	180	1000	40	6	1800	10	3	800	30	5	D	Rural
Result for the direct problem														
Station A										Station B				
$C_{p,max}$ (g/m^3)				Δt_m (s)						$C_{p,max}$ (g/m^3)				Δt_m (s)
$1.08 \cdot 10^{-2}$				538						$4.88 \cdot 10^{-3}$				874

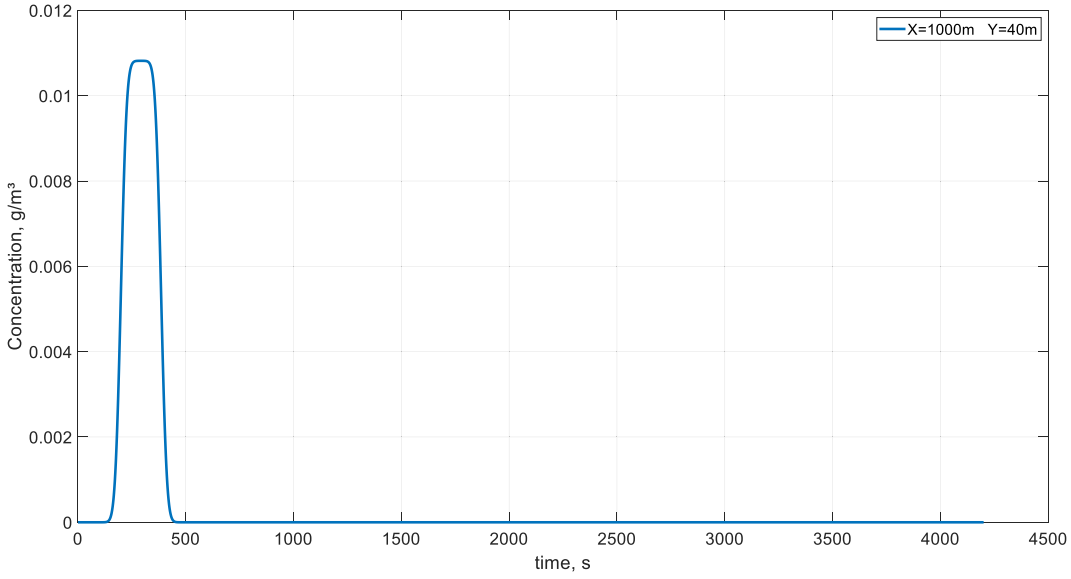

Fig. 19. Evolution of concentration at measuring station A.

xxv) Simulation of equations (3) to (7), (15) and (16) for each station. Go to step xxvi). Note that these last expressions have been obtained from equations (1) and (2).

$$\chi^{i}_{station} = \frac{2C_{p,max,station,\xi}(x,y,z,t)}{\left[\operatorname{erf}\left(\frac{x^{i}_{station,\xi}}{\sigma_x\sqrt{2}}\right) - \operatorname{erf}\left(\frac{x^{i}_{station,\xi} - V_{x,\xi}time^{i}_{station,\xi}}{\sigma_x\sqrt{2}}\right)\right]} \quad \text{for } time^{i}_{station,\xi} \le t^{*}_{r} \tag{15a}$$

$$\chi^{i}_{station} = \frac{2C_{p,max,station,\xi}(x,y,z,t)}{\left[\operatorname{erf}\left(\frac{x^{i}_{station,\xi} - V_{x,\xi}(time^{i}_{station,\xi} - t^{*}_{r})}{\sigma_x\sqrt{2}}\right) - \operatorname{erf}\left(\frac{x^{i}_{station,\xi} - V_{x,\xi}time^{i}_{station,\xi}}{\sigma_x\sqrt{2}}\right)\right]} \text{ for } time^{i}_{station,\xi} > t^{*}_{r} \tag{15b}$$

$$Q^{i}_{station,\xi} = \frac{\chi^{i}_{station} V_{x,\xi}}{g_y(x,y)\, g_z(x,z)} \tag{16}$$

xxvi) Determine the value of the following functional $\left(\phi^{i}_{Q}\right)$ giving by the expression (17) and go to step xxvii).

$$\phi^{i}_{Q} = \sum_{i=1}^{i=n} \left(Q^{i}_{A,\xi} - Q^{i}_{B,\xi}\right)^2 \tag{17}$$

xxvii) If the simulation is for the last emission source (i = n) go to step xxviii). Otherwise go to step xxiii).

xxviii) The emission source is the one that the minimum value of ϕ^{i}_{Q} and with an average rate of mass release value ($Q^{i}_{Mean,\xi}$) between the values obtained for each station ($Q^{i}_{A,\xi}$ and $Q^{i}_{B,\xi}$).

The following flow diagrams (Figs. 12 and 13) summarizes the protocol for the solution of the direct and inverse problems.

The previous steps (iv to xxviii) have been programmed in a MATLAB® work routine [17], which starts the simulation, reads the results, calculates the functionals and sets the data for the new simulation, and so on until the final solution is reached.

As we know the exact values of each variable, thanks to the direct

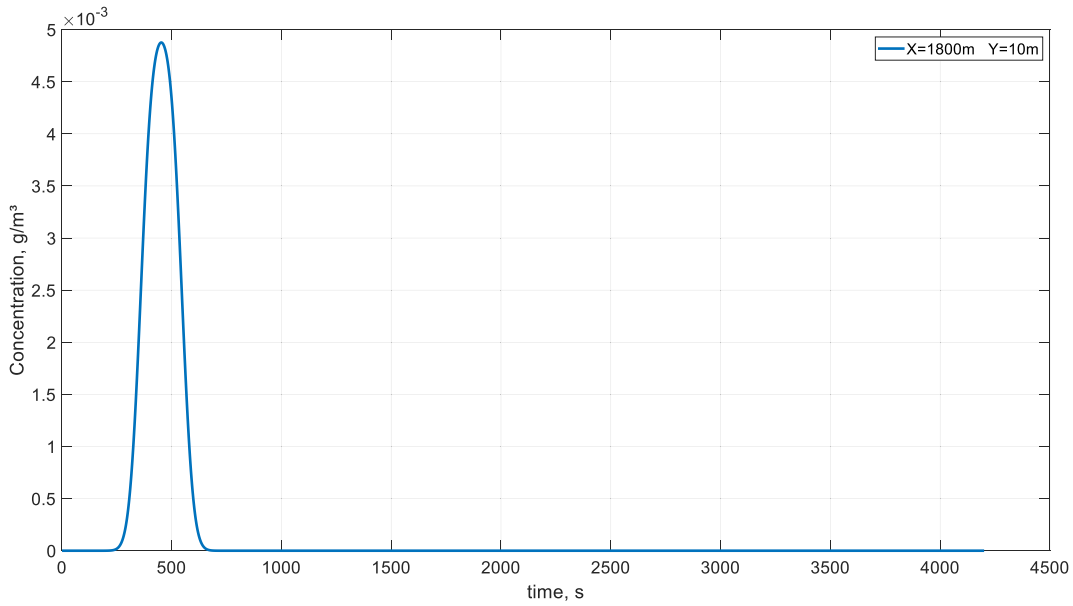

Fig. 20. Evolution of concentration at measuring station B.

Table 9
Height and distance of each of the emission sources to the measuring stations.

	Station A		Station B		h_s (m)
Source	x (m)	y (m)	x (m)	y (m)	
1	1000	10	1800	20	7
2	400	20	1200	10	9
3	1000	40	1800	10	12

problem, the verification of the results obtained with the inverse problem is immediate, expecting that the deviations obtained in the solution reached depend on the error applied to the input data.

4. Applications and verification

To verify the previous protocol, it will be applied to three different scenarios, one for each type of stability (stable, neutral and unstable). In all cases the direct problem with the input data, which we will calculate

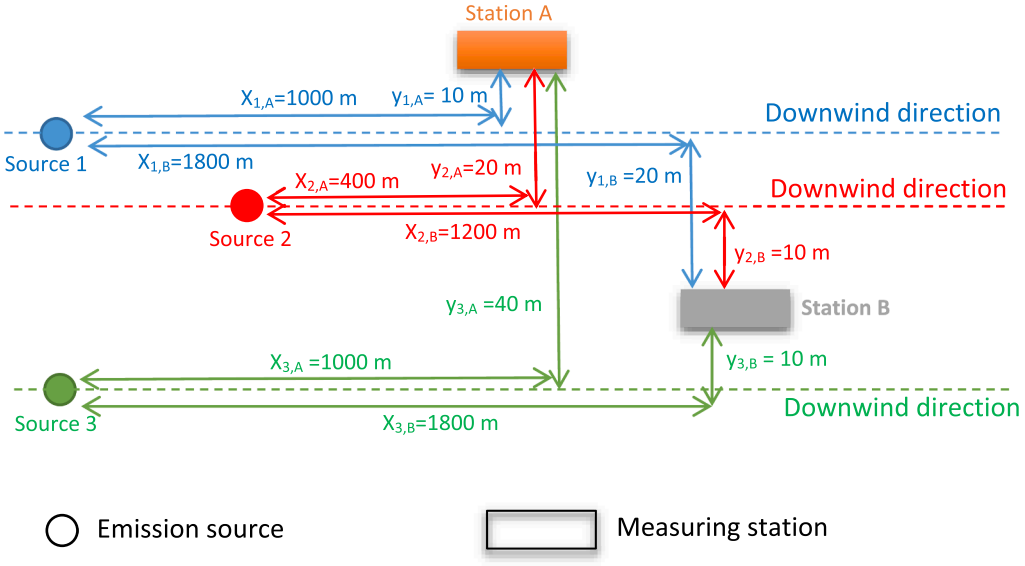

Fig. 21. Projection on the xy-plane of the determination of emission sources located at a distance $x_{A,\xi}$ (or $x_{B,\xi}$) from station A (or B) for the second scenario.

Table 10
Input data or "experimental measurements" obtained from measuring stations. Maximum error of 2%.

Station A		Station B		$\Delta x_{,\xi}$ (m)	V_x (m/s)	Atmospheric stability	Roughness
$C_{p,max,,\xi}$ (g/m^3)	$\Delta t_{m,\xi}$ (s)	$C_{p,max,,\xi}$ (g/m^3)	$\Delta t_{m,\xi}$ (s)				
$1.07{\cdot}10^{-2}$ (0.93%)	528 (1.86%)	$4.95{\cdot}10^{-3}$ (1.43%)	864 (1.14%)	798 (0.25%)	5	D	Rural

Table 11
$x^{j}_{A,\xi}$, $x^{j}_{B,\xi}$, $t_r^{*,j}$ and Ψ^{j}_{tr} for selected iterations.

Iteration	$t_r^{*,j}$ (s)	$t^{j}_{r,\xi}$ (s)	$x^{j}_{A,\xi}$ (m)	$x^{j}_{B,\xi}$ (m)	Ψ^{j}_{tr}
1	528.00	592.59	0.00	798.00	4171.62
2	264.00	273.72	778.86	1576.86	94.46
–	–	–	–	–	–
5	177.62	179.16	998.22	1796.22	2.38
6	**176.62**	**178.08**	**1000.72**	**1798.72**	**2.12**
–	–	–	–	–	–
23	**159.62**	**159.64**	**1043.04**	**1841.04**	**0.00032**

later with the inverse problem, will be solved and a maximum error of 2% will be applied to the results to obtain the "experimental measurements" or input data for the inverse problem. Although in the direct problem we know the source of emission, it is not so in the inverse problem. Thereby, in the scenarios posed for the inverse problem, although there may be more, we will assume only three possible emission sources to facilitate the understanding of the examples, since they are enough to show the protocol of the inverse problem.

4.1. First scenario

In the first scenario, an atmospheric stability class A is studied, where

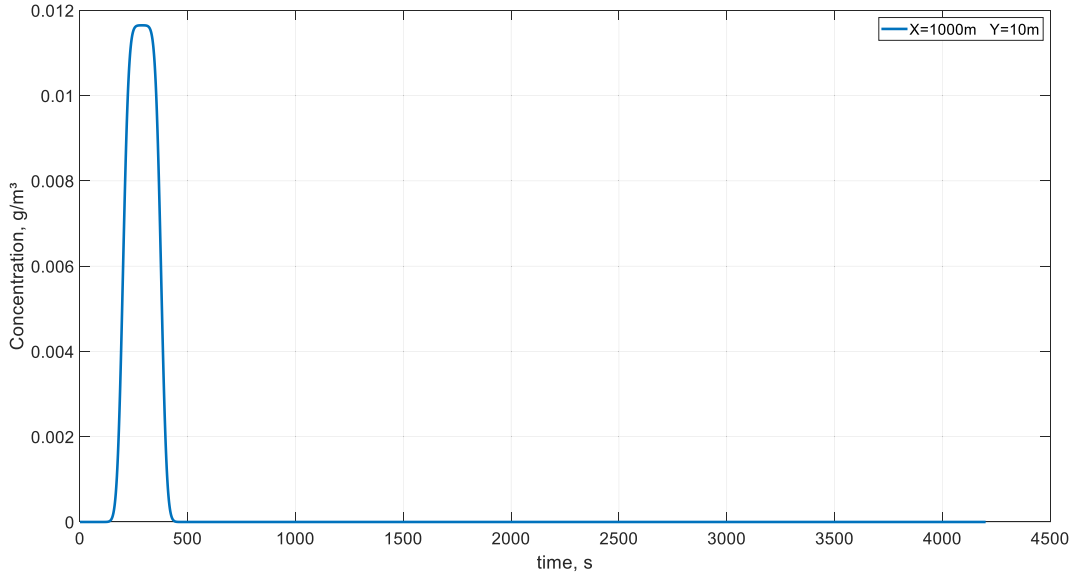

a)

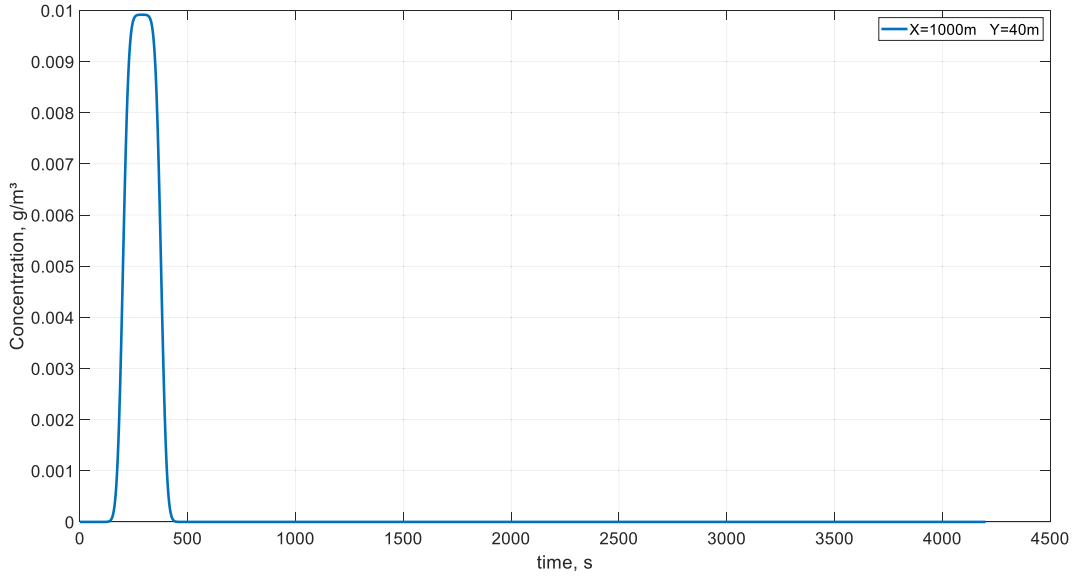

b)

Fig. 22. Evolution of concentration at measuring station A to determine the time at which the maximum concentration occurs for a) source 1 and b) source 3.

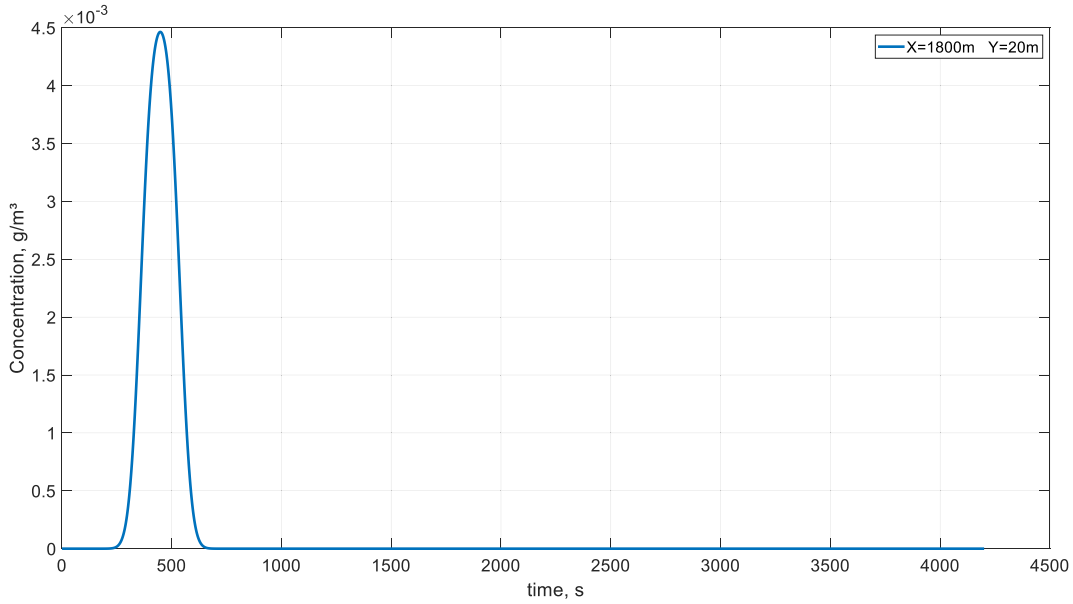

a)

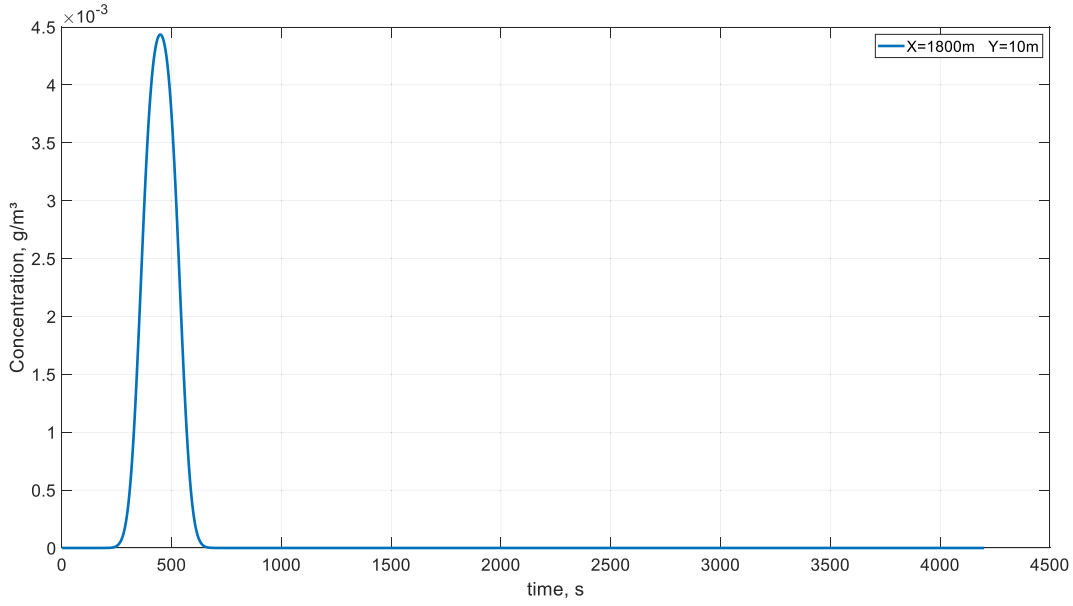

b)

Fig. 23. Evolution of concentration at measuring station B to determine the time at which the maximum concentration occurs for a) source 1 and b) source 3.

Table 12
$Q^i_{A,\xi}$, $Q^i_{B,\xi}$, ϕ^i_Q and $Q^i_{Mean,\xi}$ for sources 1 and 3.

Source	$Q^i_{A,\xi}$ (g/s)	$Q^i_{B,\xi}$ (g/s)	ϕ^i_Q	$Q^i_{Mean,\xi}$ (g/s)
1	505.19	609.90	10963.81	557.54
3	593.48	613.87	415.71	603.67

Table 2 presents the input values as well as those obtained by the simulation of the direct problem. Finally, the results at the measuring stations are shown in Figs. 14 and 15.

Table 3 and Fig. 16 show the distances from each of the possible emission sources to the measuring stations. Finally, Table 4 presents the necessary data for the inverse problem, affecting the input data and results of the direct problem by an error of up to 2%. Relative error is shown in parentheses.

Next, steps iv) to xxi) are applied until the distance values are

Table 13
Comparison between the results obtained by the direct and inverse problem.

Source	Station A			Station B			h_s (m)	Direct problem		Inverse problem	
	x (m)	y (m)	z (m)	x (m)	y (m)	z (m)		Q (g/s)	t_r (s)	Q (g/s)	t_r (s)
3	1000	40	6	1800	10	3	12	600	180	603.67 **(0.61%)**	177 **(1.67%)**

Table 14
Input data and results of the direct problem.

Input data for the direct problem														
Source				Atmospheric pollutant measuring station										Roughness
				Station A			Station B			Δx (m)	Δy (m)	V_x (m/s)	Atmospheric stability	
Number	h_s (m)	Q (g/s)	t_r (s)	x (m)	y (m)	z (m)	x (m)	y (m)	z (m)					
1	3	800	600	600	10	0	2100	20	0	1500	30	4	E	Rural

Result for the direct problem			
Station A		Station B	
$C_{p,max}$ (g/m^3)	Δt_m (s)	$C_{p,max}$ (g/m^3)	Δt_m (s)
$1.12 \cdot 10^{-1}$	926	$1.41 \cdot 10^{-2}$	1719

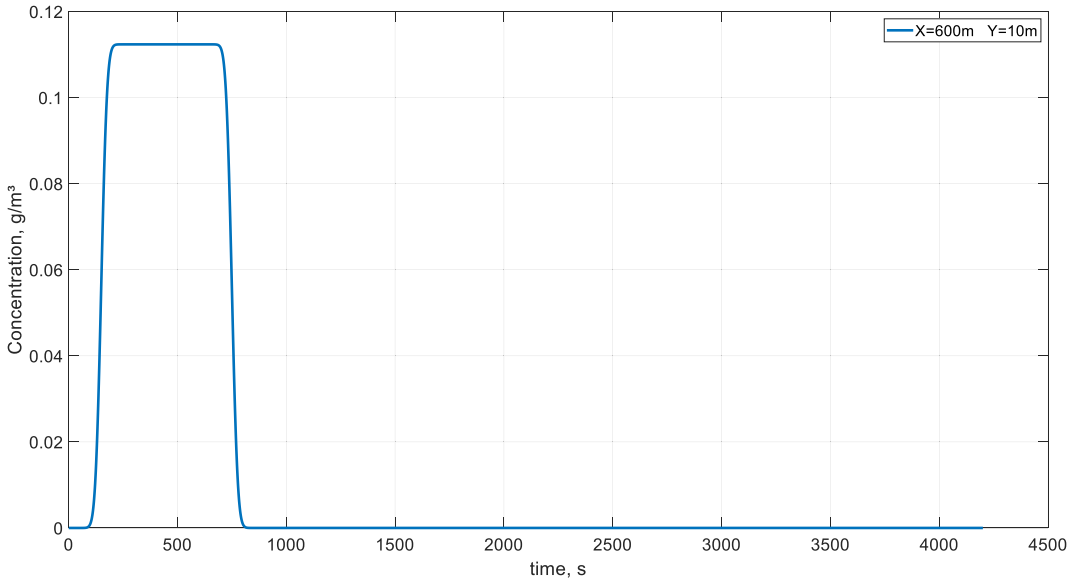

Fig. 24. Evolution of concentration at measuring station A.

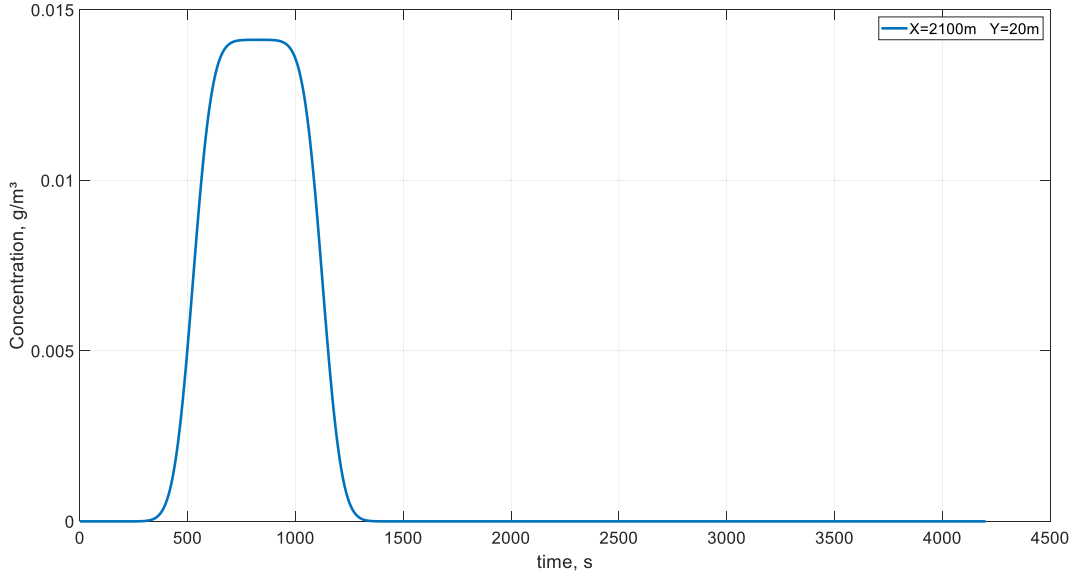

Fig. 25. Evolution of concentration at measuring station B.

Table 15
Height and distance of each of the emission sources to the measuring stations.

	Station A		Station B		h_s (m)
Source	x (m)	y (m)	x (m)	y (m)	
1	600	10	2100	20	3
2	300	15	1800	15	7
3	600	50	2100	20	9

obtained with respect to the measuring stations ($x^j_{A,\xi}$ and $x^j_{B,\xi}$) and the release time ($t_r^{*,j}$) that present the lowest functional value (Ψ^j_{tr}), Table 5.

Next, the data from iteration 23 (the one with the lowest value of the functional) are taken and the emission sources that are at a distance close to 918.53 m from station A and 1516.53 m from station B must be selected. This requirement is met by emission sources 1 and 3 that are located at a distance of 900 m from station A and 1500 m from station B. In this way, the data necessary to start the second stage are sources 1 and 3, 900 m for $x^j_{A,\xi}$, 1500 m for $x^j_{B,\xi}$ and 362 s for $t_r^{*,j}$ (the last value is obtained from iteration 12 which is the corresponding one for the previous distances).

The second stage covers steps xxii) to xxviii), where we must first determine the time at which the maximum concentration is reached for each station using a random mass rate (550 g/s). For source 1, the mentioned time is 473 and 683 s for stations A and B, respectively, and for source 3 is 433 and 680 s for A and B, respectively, Figs. 17 and 18. Finally, we can determine the emission mass rate and therefore the emission source by choosing the one that presents the lowest value for the functional ϕ^i_Q, Table 6.

If we analyze the results shown in Table 6, it is concluded that the emission occurred in source 1. Table 7 shows the comparison of the input data of the direct problem with those obtained with the inverse problem, where the relative error is shown in bold. As can be seen, the errors obtained by the inverse problem are small, being less than 2%, allowing the values of the mass rate, the position of emission source and the release time to be reliably determined.

Table 17
$x^j_{A,\xi}$, $x^j_{B,\xi}$, $t_r^{*,j}$ and Ψ^j_{tr} for selected iterations.

Iteration	$t_r^{*,j}$ (s)	$t^j_{r,\xi}$ (s)	$x^j_{A,\xi}$ (m)	$x^j_{B,\xi}$ (m)	Ψ^j_{tr}
1	932.00	921.83	0.00	1501.00	103.50
2	466.00	468.31	862.58	2363.58	5.33
–	–	–	–	–	–
11	620.05	619.75	573.90	2074.90	0.088
12	619.05	618.77	575.77	2076.77	0.077
–	–	–	–	–	–
25	**606.05**	**606.02**	**600.06**	**2101.06**	**0.001**
26	605.05	605.04	601.93	2102.93	0.00017
27	**604.05**	**604.06**	**603.80**	**2104.80**	**0.00003**

4.2. Second scenario

In the second scenario, an atmospheric stability class D is studied, where Table 8 presents the input values as well as those obtained by the simulation of the direct problem. Finally, the results at the measuring stations are shown in Figs. 19 and 20.

Table 9 and Fig. 21 show the distances from each of the possible emission sources to the measuring stations. Finally, Table 10 presents the necessary data for the inverse problem, affecting the input data and results of the direct problem by an error of up to 2%. Relative error is shown in parentheses.

Next, steps iv) to xxi) are applied until the distance values are obtained with respect to the measuring stations ($x^j_{A,\xi}$ and $x^j_{B,\xi}$) and the release time ($t_r^{*,j}$) that present the lowest functional value (Ψ^j_{tr}), Table 11.

Next, the data from iteration 23 (the one with the lowest value of the functional) are taken and the emission sources that are at a distance close to 1043.04 m from station A and 1841.04 m from station B must be selected. This requirement is met by emission sources 1 and 3 that are

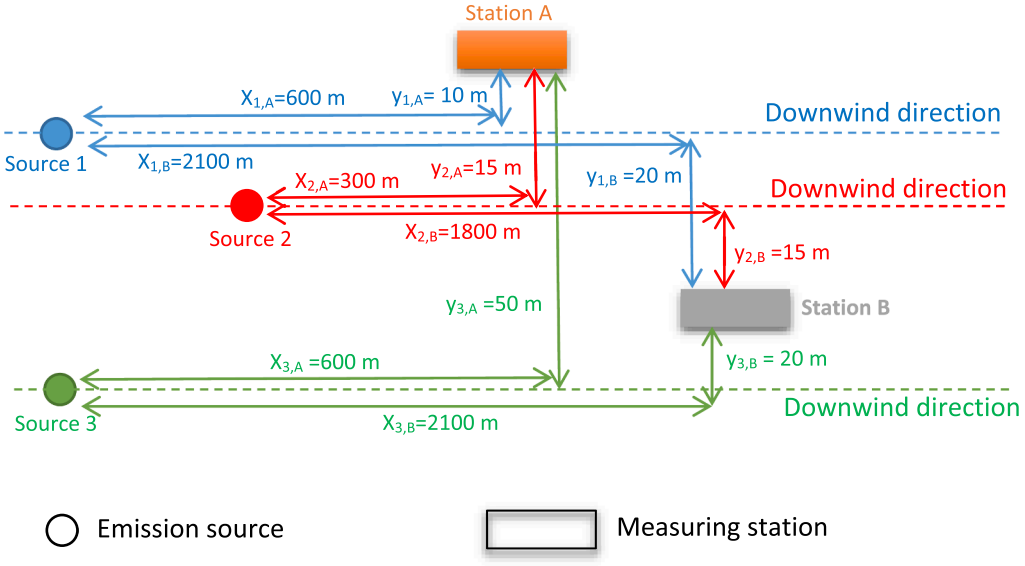

Fig. 26. Projection on the xy-plane of the determination of emission sources located at a distance $x_{A,\xi}$ (or $x_{B,\xi}$) from station A (or B) for the third scenario.

Table 16
Input data or "experimental measurements" obtained from measuring stations. Maximum error of 2%.

Station A		Station B		$\Delta x_{,\xi}$ (m)	V_x (m/s)	Atmospheric stability	Roughness
$C_{p,max,,\xi}$ (g/m^3)	$\Delta t_{m,\xi}$ (s)	$C_{p,max,,\xi}$ (g/m^3)	$\Delta t_{m,\xi}$ (s)				
$1.14{\cdot}10^{-1}$ (1.79%)	932 (0.65%)	$1.43{\cdot}10^{-2}$ (1.42%)	1726 (0.41%)	1501 (0.07%)	4	D	Rural

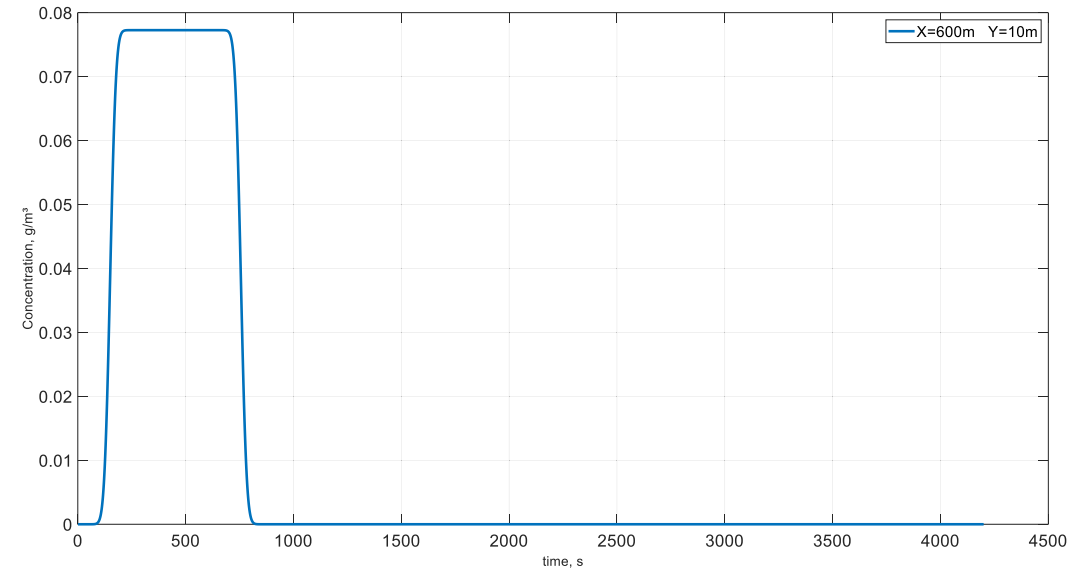

a)

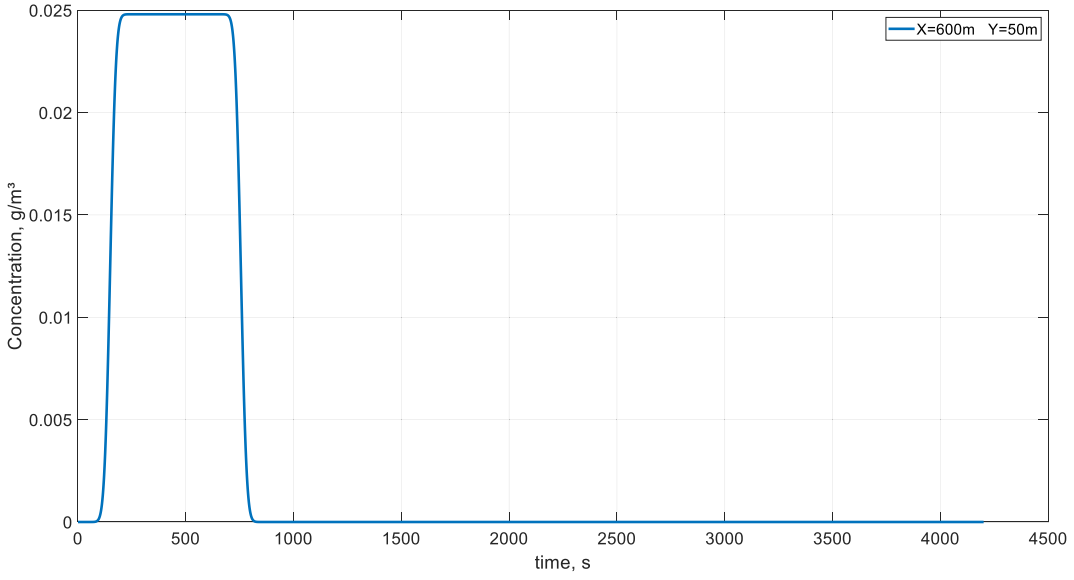

b)

Fig. 27. Evolution of concentration at measuring station A to determine the time at which the maximum concentration occurs for a) source 1 and b) source 3.

located at a distance of 1000 m from station A and 1800 from station B. In this way, the data necessary to start the second stage are sources 1 and 3, 1000 m for $x^{j}_{A,\xi}$, 1800 m for $x^{j}_{B,\xi}$ and 177 s for $t_r^{*,j}$ (the last value is obtained from iteration 18 which is the corresponding one for the previous distances).

The second stage covers steps xxii) to xxviii), where we must first determine the time at which the maximum concentration is reached for each station using a random mass rate (550 g/s). For both sources, the mentioned time is 289 and 449 s for stations A and B, respectively, Figs. 22 and 23. Finally, we can determine the emission mass rate and therefore the emission source by choosing the one that presents the lowest value for the functional ϕ^{i}_{Q}, Table 12.

If we analyze the results shown in Table 12, it is concluded that the emission occurred in source 3. Table 13 shows the comparison of the input data of the direct problem with those obtained with the inverse problem, where the relative error is shown in bold. As can be seen, the errors obtained by the inverse problem are small, being less than 2% (acceptable in engineering problems), allowing the values of the mass rate, the position of emission source and the release time to be reliably determined.

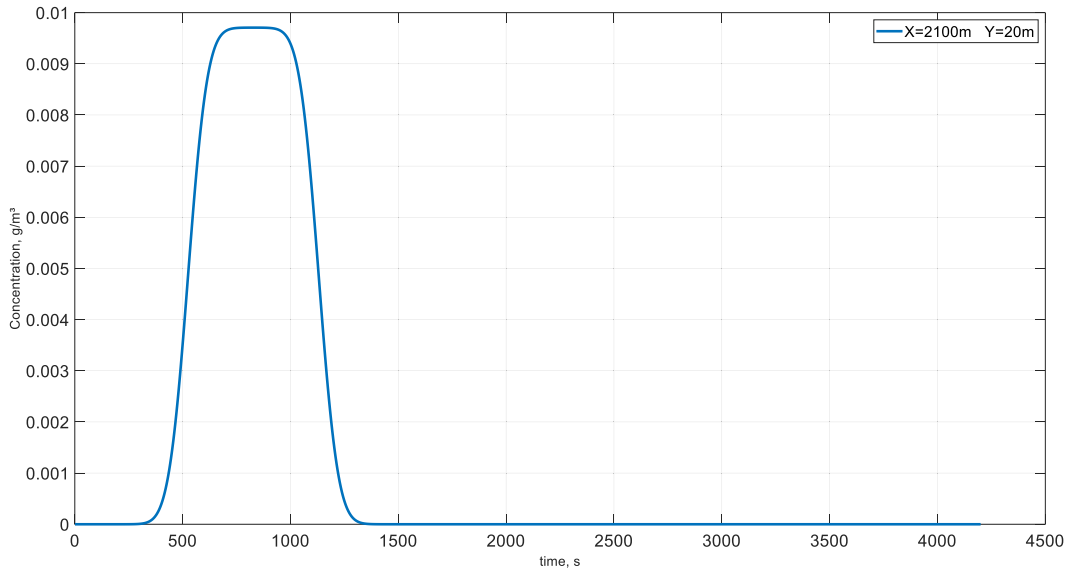

a)

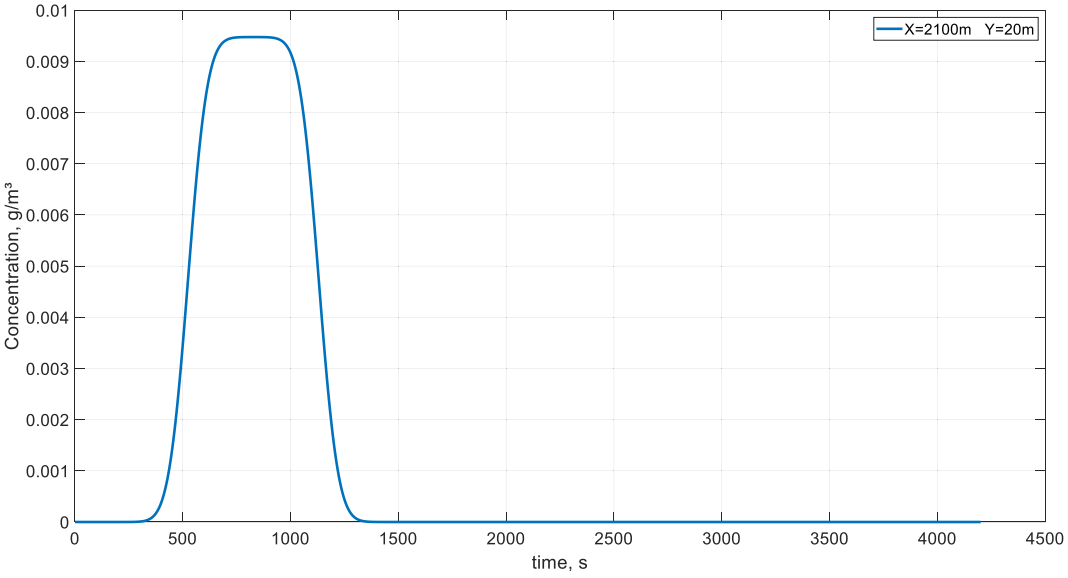

b)

Fig. 28. Evolution of concentration at measuring station B to determine the time at which the maximum concentration occurs for a) source 1 and b) source 3.

Table 18
$Q^i_{A,\xi}$, $Q^i_{B,\xi}$, ϕ^i_Q and $Q^i_{Mean,\xi}$ for sources 1 and 3.

Source	$Q^i_{A,\xi}$ (g/s)	$Q^i_{B,\xi}$ (g/s)	ϕ^i_Q	$Q^i_{Mean,\xi}$ (g/s)
1	811.55	810.24	1.71	810.89
3	2527.88	830.00	2882783.21	1678.94

4.3. Third scenario

In the last scenario, an atmospheric stability class E is studied, where Table 14 presents the input values as well as those obtained by the simulation of the direct problem. Finally, the results at the measuring stations are shown in Figs. 24 and 25.

Table 15 and Fig. 26 show the distances from each of the possible emission sources to the measuring stations. Finally, Table 16 presents the necessary data for the inverse problem, affecting the input data and results of the direct problem by an error of up to 2%. Relative error is shown in parentheses.

Next, steps iv) to xxi) are applied until the distance values are obtained with respect to the measuring stations ($x^j_{A,\xi}$ and $x^j_{B,\xi}$) and the release time ($t_r^{*,j}$) that present the lowest functional value (Ψ^j_{tr}),

Table 19
Comparison between the results obtained by the direct and inverse problem.

Source	Station A			Station B			h_s (m)	Direct problem		Inverse problem	
	x (m)	y (m)	z (m)	x (m)	y (m)	z (m)		Q (g/s)	t_r (s)	Q (g/s)	t_r (s)
1	600	10	0	2100	20	0	3	800	600	810.89 **(1.36%)**	606 **(1.00%)**

Table 17.

Next, the data from iteration 27 (the one with the lowest value of the functional) are taken and the emission sources that are at a distance close to 603.80 m from station A and 2104.80 m from station B must be selected. This requirement is met by emission sources 1 and 3 that are located at a distance of 600 m from station A and 2100 from station B. In this way, the data necessary to start the second stage are sources 1 and 3, 600 m for $x^j_{A,\xi}$, 2100 m for $x^j_{B,\xi}$ and 606 s for $t_r^{*,j}$ (the last value is obtained from iteration 69 which is the corresponding one for the previous distances).

The second stage covers steps xxii) to xxviii), where we must first determine the time at which the maximum concentration is reached for each station using a random mass rate (550 g/s). For source 1, the mentioned time is 456 and 827 s for stations A and B, respectively, and for source 3 is 454 and 829 s for A and B, respectively, Figs. 27 and 28. Finally, we can determine the emission mass rate and therefore the emission source by choosing the one that presents the lowest value for the functional ϕ^i_Q, Table 18.

If we analyze the results shown in Table 18, it is concluded that the emission occurred in source 1. Table 19 shows the comparison of the input data of the direct problem with those obtained with the inverse problem, where the relative error is shown in bold. As can be seen, the errors obtained by the inverse problem are small, being less than 1.5%, allowing the values of the mass rate, the position of emission source and the release time to be reliably determined.

For the three cases studied, which include each of the atmospheric stabilities, the proposed methodology can determine the possible emission source, as well as the pollutant release time and the rate of mass release with relatively small errors.

5. Application of the proposed inverse problem to other pollutant diffusion software

The inverse problem proposed in this work is valid for other contaminant diffusion software, such as those that implement the phenomena of diffusion, drag, turbulence, etc. [1–3]. The use of the equations given by the NOAA for both the direct and the inverse problem is due to the fact that they are included in software of recognized prestige from the U.S. Environmental Protection Agency (U.S. E.P.A) [10]. For the implementation of the proposed protocol for the inverse problem in other software, the steps described below must be followed. i) The first stage procedure of the inverse problem is followed using expressions (8) to (11) given in this article, which allows calculating both the release time and the distances from the emission source to the measuring stations. Equations (9) to (11) can be adjusted again for the software used following the method specified in subsection 2.2. ii) The procedure of the second stage is followed with the software used to calculate the rate of mass release. Depending on the software a simple iterative process may be needed for step xxv).

6. Contributions and conclusions

The protocol proposed for the inverse problem allows the determination of the three main parameters that control the contaminant dispersion released from a gas emission source, namely position, release time and rate of mass release (source position, t_r and Q), providing convergent and very precise, and therefore, reliable results, even for experimental measurements affected by errors of up to 2%. Determining these parameters is a fundamental aim in knowing the position of the source and the amount of neutrally-buoyant pollutants when a short duration emission occurs. Furthermore, in order to implement the inverse protocol, it is necessary to define a new coefficient, which we have called coefficient of dispersion deformation (δ), that relates the effect of dispersion in the measurement time of a pollutant, the distance in the downwind direction and the atmospheric stability categories. This coefficient, which has been developed by applying dimensional characterization techniques, only depends on the distance to the source in the downwind direction, since the other two directions mainly affect the concentration and its influence on the measurement time of the station is practically negligible. The procedure for obtaining the aforementioned coefficient, equations (8) to (11), has been validated by means of a sensitivity analysis, where the sensitivity coefficients confirmed the expressions obtained.

The actions of the protocol of the inverse problem, which have been programmed with a Matlab® work routine [17] and which include steps iv) to xxviii) (Fig. 13), are divided into two well-differentiated stages. In the first, the simulations are started for each iteration, the functionals are calculated to program the next iteration, setting the new values of measurement time and the distance of the emission source in downwind direction with respect to the measuring stations by comparing the simulated and experimental values, and so on until reaching the final solution. In the second, an analogous procedure is followed until the mass rate and the emission source position is obtained.

As expected, the results obtained have been affected by the errors of the experimental measurements of pollutant concentrations, position, and time that the station has been measuring the pollutant, since they are the input data of the inverse problem. However, it should be noted that despite the fact that the measurements had errors of up to 2% (a value that can be considered appreciable), for the cases studied, very precise solutions have been obtained. In relation to the position, the protocol allows to determine the source of emission since initially we know the possible emission sources. Regarding the rate of mass release (Q), the deviations in the results are less than 2% for errors in the experimental measurements of up to 2% for the cases studied. Finally, in relation to pollutant release time, the deviations are less than 2% for errors in experimental measurements of up to 2%. It should be noted that in scenarios 1 and 3 the error is equal to or less than 1%. The explanation that scenario 2 shows a greater error is due to the fact that in this case the pollutant release time is small, producing a greater relative error for the same absolute error. As we have already mentioned before, these results can be considered very successful in this field of engineering.

The proposed protocol for the inverse problem has been successfully verified following the procedure described below. From the numerical simulation (direct problem) the pollutant concentration values and time that the station has been measuring the pollutant for two measuring stations are obtained. Affecting these variables with a random relative error (up to 2%), an inverse protocol is applied to recover the initial parameters of the problem with a successful result. The numerical simulations have been performed with Matlab® [17] implementing the

complete mathematical model given by NOAA for the ALOHA software [10].

Declaration of Competing Interest

The authors declare that they have no known competing financial interests or personal relationships that could have appeared to influence the work reported in this paper.

References

[1] ASHRAE (American Society of Heating Refrigeration and Air-conditioning Engineers), Building air intake and exhaust design, in: ASHRAE Handbook Heating, Ventiating and Air-conditioning Applications, Atlanta (USA): ASHRAE, 2007.

[2] M. Lateb, R.N. Meroney, M. Yataghene, H. Fellouah, F. Saleh, M.C. Boufadel, On the use of numerical modelling for near-field pollutant dispersion in urban environments - A review, Environ. Pollut. (2016), https://doi.org/10.1016/j.envpol.2015.07.039.

[3] J.F. Sánchez-Pérez, M.R. Mena-Requena, M. Cánovas, Mathematical Modeling and Simulation of a Gas Emission Source Using the Network Simulation Method, Mathematics 8 (11) (2020) 1996, https://doi.org/10.3390/math8111996.

[4] O.F.T. Roberts, The theoretical scattering of smoke in a turbulent atmosphere, in: Proceedings of the Royal Society of London. Series A, Containing Papers of a Mathematical and Physical Character, 1923, doi: 10.1098/rspa.1923.0132.

[5] O.G. Sutton, A theory of eddy diffusion in the atmosphere, Proc. Royal Soc. A 135 (1932) 143–165, https://doi.org/10.1098/rspa.1932.0025.

[6] G.D.R., Micrometeorology. By O. G. Sutton. New York (McGraw-Hill), 1953. Pp. xii, 333; 35 Figs., 30 tables. 61s, Quart. J. Royal Meteorol. Soc., 1953, doi: 10.1002/qj.49707934125.

[7] F. Pasquill, Atmospheric Dispersion Models for Environmental Pollution Applications, in: Lectures on Air Pollution and Environmental Impact Analyses, American Meteorological Society, Boston, USA, 1982, https://doi.org/10.1007/978-1-935704-23-2_2.

[8] Meteorology and atomic energy 1968. D. H. Slade (Ed.). Air Resources Laboratory, ESSA, for USAEC Division of Technical Information. Pp. ×, 445; 234 Figures; 60 Tables. $3, Quart. J. Royal Meteorol. Soc., 1969, doi: 10.1002/qj.49709540423.

[9] D.B. Turner, A Diffusion Model for an Urban Area, J. Appl. Meteorol. (1964), https://doi.org/10.1175/1520-0450(1964)003<0083:admfau>2.0.co;2.

[10] R. Jones, W. Lehr, D. Simecek-Beatty, R.M. Reynolds, ALOHA ® (AREAL LOCATIONS OF HAZARDOUS ATMOSPHERES) 5.4.4. Washington, USA: U.S. DEPARTMENT OF COMMERCE, 2013.

[11] WHO, Ambient (outdoor) air pollution, https://www.who.int/en/news-room/fact-sheets/detail/ambient-(outdoor)-air-quality-and-health, 2018.

[12] J.F. Sanchez Perez, M. Conesa, I. Alhama, Solving ordinary differential equations by electrical analogy: A multidisciplinary teaching tool, Eur. J. Phys. (2016), https://doi.org/10.1088/0143-0807/37/6/065703.

[13] E. Palazzi, M. De Faveri, G. Fumarola, G. Ferraiolo, Diffusion from a steady source of short duration, Atmos. Environ. 16 (12) (1982) 2785–2790, https://doi.org/10.1016/0004-6981(82)90029-4.

[14] S.R. Hanna, Handbook on atmospheric diffusion models, 1981.

[15] G. A. Briggs, Diffusion estimation of small emissions, Contribution No.79, Atmospheric Turbulence and Diffusion Laboratory 1973 Annual Report. 1973.

[16] G.A. Beals, A guide to local dispersion of air pollutants, 1971.

[17] Matlab software. [Online]. Available: https://es.mathworks.com/products/matlab.html.

[18] M. Conesa, J.F. Sánchez Pérez, I. Alhama, F. Alhama, On the nondimensionalization of coupled, nonlinear ordinary differential equations, Nonlinear Dyn. (2016), https://doi.org/10.1007/s11071-015-2233-8.

[19] J.F. Sánchez Pérez, M. Conesa, I. Alhama, F. Alhama, M. Cánovas, Searching fundamental information in ordinary differential equations. Nondimensionalization technique, PLoS ONE (2017), https://doi.org/10.1371/journal.pone.0185477.

[20] J.F. Sánchez-Pérez, M. Conesa, I. Alhama, M. Cánovas, Study of Lotka-Volterra biological or chemical oscillator problem using the normalization technique: Prediction of time and concentrations, Mathematics (2020), https://doi.org/10.3390/MATH8081324.

[21] F. Alhama López, C.N. Madrid García, Analisis dimensional discriminado en mecanica de fluidos y transferencia de calor, 1st ed. Cartagena: Reverté, 2011.

[22] J.F. Sánchez-Pérez, I. Alhama, Universal curves for the solution of chlorides penetration in reinforced concrete, water-saturated structures with bound chloride, Commun. Nonlinear Sci. Numer. Simul. 84 (2020), https://doi.org/10.1016/j.cnsns.2020.105201.

[23] E.G. Ferradás, F.D. Alonso, J.F. Sánchez Pérez, A.M. Aznar, J.R. Gimeno, J.M. Alonso, Characteristic overpressure–impulse–distance curves for vessel burst, Process Safety Progress, 25(3) (Sep. 2006) 250–254. doi: 10.1002/PRS.10140.

[24] F. Díaz Alonso, E. González Ferradás, J. F. Sánchez Pérez, A. Miñana Aznar, J. Ruiz Gimeno, and J. Martínez Alonso, Consequence analysis by means of characteristic curves to determine the damage to humans from the detonation of explosive substances as a function of TNT equivalence, J. Loss Prev. Process Industries 20(3) (May 2007) 187–193. doi: 10.1016/J.JLP.2007.03.003.

[25] Lee, Lees' Loss Prevention in the Process Industries: Hazard Identification, Assessment And Control: Fourth Edition, vol. 1–2. 2012. doi: 10.1016/C2009-0-24104-3.

[26] J.V. James, V. Beck, Ben. Blackwell, C.R. st. Clair, Inverse heat conduction: ill-posed problems, p. 308, 1985.

[27] B. Heinrich, B. Hofmann, Beck, J. V.; Blackwell, B.; St. Clair, C. R., jr., Inverse Heat Conduction. Ill-Posed Problems. New York etc., J. Wiley & Sons 1985. XVII, 308 S., £ 46.00. ISBN 0-471-08319-4, ZAMM - Journal of Applied Mathematics and Mechanics / Zeitschrift für Angewandte Mathematik und Mechanik, vol. 67, no. 3, pp. 212–213, Jan. 1987, doi: 10.1002/ZAMM.19870670331.

[28] O.M. Alifanov, E.A. Artyukhin, S.V. Rumyantsev, Extreme Methods for Solving III-posed Problems with Applications to inverse Heat Transfer Problems. Begell House Inc., 1995.

[29] J. Zueco, F. Alhama, Inverse estimation of temperature dependent emissivity of solid metals, J. Quant. Spectrosc. Radiat. Transf. 101(1) (2006). doi: 10.1016/j.jqsrt.2005.11.005.

[30] B. Lamien, et al., A Bayesian approach for the estimation of the thermal diffusivity of aerodynamically levitated solid metals at high temperatures, Int. J. Heat Mass Transf. 141 (2019), https://doi.org/10.1016/j.ijheatmasstransfer.2019.06.054.

[31] D. Calvetti, J.P. Kaipio, E. Somersalo, Inverse problems in the Bayesian framework, Inverse Probl. 30(11) (2014). doi: 10.1088/0266-5611/30/11/110301.

[32] I. Alhama, M. Cánovas, F. Alhama, On the nondimensionalization process in complex problems: Application to natural convection in anisotropic porous media, Math. Probl. Eng. 2014 (2014), https://doi.org/10.1155/2014/796781.

[33] G. García-Ros, I. Alhama, M. Cánovas, F. Alhama, Derivation of universal curves for nonlinear soil consolidation with potential constitutive dependences, Math. Probl. Eng. 2018 (2018), https://doi.org/10.1155/2018/5837592.

[34] G. García-Ros, I. Alhama, M. Cánovas, Use of discriminated nondimensionalization in the search of universal solutions for 2-D rectangular and cylindrical consolidation problems, Open Geosci. 10(1) (2018). doi: 10.1515/geo-2018-0016.

[35] J.F. Sánchez-Pérez, I. Alhama, Simultaneous determination of initial porosity and diffusivity of water-saturated reinforced concrete subject to chloride penetration by inverse problem, Constr. Build. Mater. (2020), https://doi.org/10.1016/j.conbuildmat.2020.120412.

[36] J. Zueco, F. Alhama, Inverse estimation of temperature dependent emissivity of solid metals, J. Quant. Spectrosc. Radiat. Transfer (2006), https://doi.org/10.1016/j.jqsrt.2005.11.005.

[37] G. García-Ros, I. Alhama, Method to determine the constitutive permeability parameters of non-linear consolidation models by means of the oedometer test, Mathematics 8 (12) (2020) 1–19, https://doi.org/10.3390/math8122237.

[38] M. Matsumoto, T. Nishimura, Mersenne Twister: A 623-Dimensionally Equidistributed Uniform Pseudo-Random Number Generator, ACM Trans. Model. Comput. Simul. 8(1) (1998). doi: 10.1145/272991.272995.